AGU PUBLICATIONS

Journal of Advances in Modeling Earth Systems

RESEARCH ARTICLE

10.1002/2015MS000621

Key Points:
- The Ensemble Cumulus Parameterization includes multiple closures with varying weights specific of land and ocean
- It allows a systematic, objective evaluation of how varying cumulus closures affect regional climate simulations
- Cumulus closures greatly affect the model ability in capturing spatiotemporal variations of U.S. coastal ocean precipitation

Supporting Information:
- Supporting Information S1

Correspondence to:
X.-Z. Liang,
xliang@umd.edu

Citation:
Qiao, F., and X.-Z. Liang (2016), Effects of cumulus parameterization closures on simulations of summer precipitation over the United States coastal oceans, *J. Adv. Model. Earth Syst.*, *8*, 764–785, doi:10.1002/2015MS000621.

Received 2 JAN 2016
Accepted 21 APR 2016
Accepted article online 30 APR 2016
Published online 27 MAY 2016

Effects of cumulus parameterization closures on simulations of summer precipitation over the United States coastal oceans

Fengxue Qiao[1,2] and Xin-Zhong Liang[2,3,4]

[1]Key Laboratory of Geographic Information Science, Ministry of Education, East China Normal University, Shanghai, China, [2]Department of Atmospheric Sciences, University of Illinois at Urbana-Champaign, Champaign, Illinois, USA, [3]Earth System Science Interdisciplinary Center, University of Maryland, College Park, Maryland, USA, [4]Department of Atmospheric and Oceanic Science, University of Maryland at College Park, College Park, Maryland, USA

Abstract This study evaluates the effects of major cumulus parameterization closures on summer precipitation simulations over the U.S. Atlantic Coasts and Gulf of Mexico. A series of mesoscale regional climate model simulations using an Ensemble Cumulus Parameterization (ECP) that incorporates multiple alternate closure schemes into a single cloud model formulation are conducted and compared to determine the systematic errors and relative performances of individual and combined closures in capturing precipitation spatiotemporal variations. The results show that closure algorithms largely affect precipitation's geographic distribution, frequency and intensity, and diurnal cycle. The quasi-equilibrium and total instability adjustment closures simulate widespread wet biases, while the instability tendency closure produces systematic dry biases. Two closure algorithms based on the average vertical velocity at the cloud base and column moisture convergence complementarily reproduce the observed precipitation pattern and amount, and capture the frequency of heavy rainfall events better than other closures. In contrast, the instability tendency closures are better at capturing the diurnal phase but yield much larger deficits in amount. Therefore, cloud base vertical velocity and moisture convergence may be the primary factors controlling precipitation seasonal mean and daily variation, while the instability tendency may play a critical role in regulating the diurnal cycle phase.

1. Introduction

Precipitation modeling involves many coupled processes between cumulus convection, cloud microphysics, the planetary boundary layer, land and ocean surface, and radiation [*Dai*, 2006; *Liang et al*., 2012]. Among these interactions, cumulus convection plays a central role in regulating precipitation prediction, especially during the midlatitude summer and in the tropics when convection is most active [*Arakawa*, 2004; *Liang et al*., 2007]. However, there are no universally accepted formulations or assumptions for cumulus parameterizations (CUPs) to accurately represent the subgrid convective processes in current general circulation models (GCMs) and regional climate models (RCMs) [*Gochis et al*., 2002; *Yano et al*., 2013]. The CUPs often differ in closure assumptions, trigger functions and cloud models, leading to large discrepancies in simulating convective and thus total precipitation [*Grell and Dévényi*, 2002; *Arakawa*, 2004].

Many studies have demonstrated that precipitation modeling over oceans, especially in the tropics, is highly sensitive to CUPs [*Zhang and McFarlane*, 1995; *Maloney and Hartmann*, 2001; *Dai*, 2006; *Lin*, 2007]. In particular, CUP deficiencies have been associated with some persistent model errors in geographic distribution of precipitation seasonal mean, frequency and intensity, and diurnal cycle. For instance, GCMs tend to produce unrealistic double intertropical convergence zones (ITCZ) straddling the equator across much of the Pacific [e.g., *Wu et al*., 2003; *Zhang and Wang*, 2006; *Li and Xie*, 2014]. Many studies have attributed this error to unrealistic sea surface temperature prediction associated with deep convection initiation and model deficiencies in CUPs, though the cause of this so-called double ITCZ problem is complex. Another challenge is that models generally overestimate the occurrence of light rain, but underestimate the frequency and intensity of heavy precipitation [*Dai*, 2006]. This implies that CUPs produce convective activity too often and/or convert atmospheric moisture to rainfall too fast [*Sun et al*., 2006]. In addition, many models have difficulties realistically reproducing the observed diurnal cycle over both land and oceans [e.g., *Bechtold et al*., 2004; *Dai*, 2006]. It is widely recognized that modeled rainfall often peaks too early during the daytime [*Dai and*

Trenberth, 2004; *Liang et al*., 2004a], indicating that CUPs are responding too rapidly to surface flux variations either caused by problems in deep convective triggering mechanisms or by convective mixing/entrainment deficiencies [*Bechtold et al*., 2004].

Many efforts have been made to reduce these model precipitation biases over oceans by improving the cumulus closure assumption, as it is the fundamental component of CUPs [*Arakawa*, 2004]. The closure determines the location and intensity of convection [*Grell and Dévényi*, 2002] and has been proven to significantly affect precipitation amounts and frequency over oceans. For instance, *Zhang and Mu* [2005] revised the cumulus closure of *Zhang and McFarlane* [1995] to base it on the large-scale forcing in the free troposphere rather than the convective available potential energy (CAPE) in the whole atmosphere. This revision greatly reduced the dry bias in the western Pacific monsoon region and also significantly mitigated the double ITCZ problem by reducing the warm bias in the southern ITCZ region and the cold bias in the cold tongue over the equator [*Zhang and Wang*, 2006]. *Wilcox and Donner* [2007] also found that the closure in the *Donner* [1993] cumulus scheme which assumes convections to balance the increase rate of large-scale instability above the boundary layer plays an important role in realistically simulating heavy rainfall frequency distributions. A few studies have focused on the effects of refined cumulus closures representing equilibrium and nonequilibrium convection in large-scale models on the diurnal cycle of convection over the continental U.S. [e.g., *Zhang*, 2003]. Given that convective systems over oceans generally have different structures and life cycles from those over land [*Sato et al*., 2009], the question of how cumulus closure affects the diurnal cycle of convection and precipitation over oceans remains unanswered.

Current CUP schemes are generally based on several major closure assumptions, including the integrated moisture convergence assumption [e.g., *Kuo*, 1974], the vertical advection of moisture assumption [e.g., *Krishnamurti et al*., 1983], the widely used quasi-equilibrium assumption proposed by *Arakawa and Schubert* [1974], and the environmental low-level wind convergence closure designed by *Frank and Cohen* [1987]. These closure assumptions are highly sensitive to model resolution and their resulting responses are quite case dependent [*Molinari and Dudek*, 1992]. However, very few studies can systematically identify the validity of these closure assumptions because CUPs are extremely complex, containing not only different formulations for a specific closure but also many other variable parameters [*Grell*, 1993]. As such, large uncertainties exist regarding the applicability and performance of these cumulus closures for weather forecasts or climate prediction [*Arakawa*, 2004; *Fletcher and Bretherton*, 2010; *Qiao and Liang*, 2015; F. Qiao and X. Z. Liang, Effects of cumulus parameterization closures on summer precipitation prediction over the continental United States, submitted to *Climate Dynamics*, 2015].

Therefore, the main purpose of this study is to fully examine the effects and relative performances of cumulus closure assumptions on summer precipitation simulation over oceans by using an Ensemble Cumulus Parameterization (ECP) scheme in the Regional Climate-Weather Research and Forecasting (CWRF) model [*Liang et al*., 2012]. This ECP scheme is developed on the basis of the G3 scheme [*Grell and Dévényi*, 2002] with numerous improvements. In particular, the ECP scheme not only includes multiple cumulus closures with relative weights but also allows the selection of different closure options over the land and oceans. Applying the identical ECP scheme provides an opportunity to evaluate the regional climate prediction sensitivity specific to varying cumulus closures. The sensitivity analysis will be focused on the U.S. coastal oceans in summer for three key precipitation characteristics: geographic distribution, frequency and intensity, and the diurnal cycle.

The U.S. coastal oceans of most concern to this study are the Atlantic Coast and the Gulf of Mexico because they are significantly affected by hurricanes or tropical storms and their associated storm-surge floods and waves could pose severe threats to the people along the shorelines [*Maloney and Hartmann*, 2001]. Additionally, precipitation and its variability over the U.S. Atlantic Coast controls the freshwater delivery, influences the location and intensity of the sinking branch of Atlantic meridional overturning circulation, and consequently has potential effects on the Northern Hemisphere climate [*Sutton and Hodson*, 2007]. While GCMs usually capture the seasonal or annual mean precipitation patterns over the U.S. coastal oceans, they generally simulate insufficient amounts [*Kuwano-Yoshida et al*., 2010]. RCMs, on the other hand, are more sensitive to the choice of CUP. For instance, the *Grell* [1993] cumulus scheme produces dry bias, but the Kain-Fritsch scheme [*Kain and Fritsch*, 1993] yields excessive amounts [*Liang et al*., 2004b, 2012]. This study will investigate the sensitivity of CWRF, a state-of-the-science RCM, to CUPs, focusing on the relative performance of major cumulus closures in capturing spatiotemporal variations of coastal ocean precipitation.

Table 1. The CWRF Model Control Configurations of Physics Components

Domain	United States & Adjacent, centered at (37.5°N, 95.5°W) Horizontal resolution: 30 km (196 × 139) Vertical resolution: 36 levels, top at 50 hPa Buffer zone width: 14 grids (420 km)
Physics Configuration	
Cloud	XRL (Xu-Randall-Liang cloud cover parameterization) [*Xu and Randall*, 1996, *Liang et al*., 2004b]
Aerosol	MISR (Multiangle Imaging Spectroradiometer) [*Kahn et al*., 2005]
Radiation	GSFC (NASA Goddard Space Flight Center) [*Chou and Suarez*, 1999] as implemented by Liang
Surface	CSSP (Conjunctive Surface-Subsurface Process Model) [*Choi and Liang*, 2010]
PBL	CAM (NCAR Community Atmosphere Model) + ORO (Module for orographic turbulence stress and gravity wave drag) [*Rontu*, 2006]
Deep cumulus	ECP (Ensemble Cumulus Parameterization modified from G3) [*Grell and Dévényi*, 2002]
Shallow cumulus	UW (University of Washington) [*Park and Bretherton*, 2009]
Microphysics	GSFCGCE (Goddard Cumulus Ensemble Model) [*Tao et al*., 2003]
Ocean	UOM (upper ocean model) [*Ling et al*., 2015]

This paper is organized as follows. Section 2 describes the CWRF model formulation and observational data. Section 3 illustrates the details of the ECP schemes used in the study, and section 4 describes the model experiments using different cumulus closure assumptions. Section 5 presents the results, including the sensitivity of U.S. coastal ocean summer precipitation to the ECP cumulus closures with respect to precipitation spatial pattern, frequency and intensity, and diurnal cycle. The major questions addressed are as follows: (1) How do different closure algorithms affect the U.S. coastal ocean precipitation simulation regarding the above three key features? (2) Are there any promising closures that most realistically reproduce all the precipitation variations or complementarily capture certain precipitation features for further optimization? Section 6 explores possible causes of model discrepancies among these cumulus closures in terms of cloud base mass flux, convective-to-total precipitation ratio, and associated thermodynamic and large-scale circulation characteristics. Section 7 gives concluding remarks, including a preliminary attempt to improve the ECP scheme based on an ensemble of two promising cumulus closures with refined weights.

2. Model Description and Observational Data

CWRF was developed on the basis of the Weather Research and Forecasting model v3.1.1 [*Skamarock et al*., 2008] with numerous improvements of physical processes that are essential to climate scales, including interactions among land-atmosphere-ocean, convection-microphysics, and cloud-aerosol-radiation [*Liang et al*., 2012; *Liang and Zhang*, 2013; *Choi et al*., 2013; *Qiao and Liang*, 2015]. Table 1 summarizes the key physics configuration for the current CWRF control version used in this study. This includes the ECP scheme that incorporates the five types of closure assumptions most commonly used in convective parameterizations, each containing different algorithms with varying relative weights over land and oceans [*Liang et al*., 2012; *Qiao and Liang*, 2015; Qiao and Liang, submitted manuscript, 2015]. More details about these individual closure assumptions are provided in section 3.

The CWRF computation domain is centered at (37.5°N, 95.5°W) using the Lambert conformal map projection. It covers the whole continental U.S. and adjacent oceans with 30 km horizontal grid spacing, with total grid points of 196 (west-east) × 139 (south-north). There are 36 vertical levels with refined resolutions near the surface to improve the planetary boundary layer and convection representation. Over oceans, CWRF incorporates observed daily sea surface temperature (SST) variations derived from weekly analysis data (1° × 1°, 1981 November to present) [*Reynolds et al*., 2002] using conservative spline fit [*Liang et al*., 2004b]. A 2-D multilevel upper ocean model (UOM) is included in the CWRF to resolve transient air-sea interactions that essentially determine SST diurnal cycle and daily variation [*Ling et al*., 2015].

The lateral boundary conditions for CWRF are constructed from the European Centre for Medium-Range Weather Forecasts Reanalysis-Interim data (ERI) [*Dee et al*., 2011]. For model evaluation, the Tropical Rainfall Measuring Mission (TRMM) 3-hourly and daily product (3B42 version 7, 50°S–50°N, 0.25° grids, 1998–2009) is mapped onto the CWRF 30 km grids using bilinear spatial interpolation. In addition, the TRMM 3A25 monthly mean product based on Precipitation Radar measurements (37°S–37°N, 0.5° grids) [*Iguchi et al*., 2000] is adopted to distinguish observed convective and stratiform precipitation.

3. Ensemble Cumulus Parameterization Description

The ECP scheme was modified from the G3 scheme parameterizing convection through an ensemble of cumulus closures [*Grell and Dévényi*, 2002]. It is a mass-flux-based parameterization, in which *dynamic control* depicts the environment's modulation of convection using closure assumptions to relate with large-scale processes, *static control* contains various parameters and assumptions to calculate the unresolvable cloud properties, and *feedback* determines the modification of the environment by the convection via compensatory subsidence and detrainment processes. Under this same framework, multiple dynamic closure assumptions and various static control assumptions are combined to form a large suite of convective cloud members. All cloud members are run at each grid box for each time step and their results are averaged to feed back on the environment for next step of integration. Thus, the parameterization is characterized as a physical and dynamical ensemble approach.

The ECP and G3 schemes differ in three main aspects. First, the ECP scheme incorporates five major assumptions with 16 varying algorithms for *dynamic control*, while the G3 scheme uses different algorithms and contains only four types of closures, excluding the widely used quasi-equilibrium assumption. Including this popular assumption in ECP allows sensitivity analyses to better understand systematic precipitation errors in many models that use CUPs with this closure type. Second, while the G3 scheme uses equal weights for all closures, the ECP scheme adds options to specify relative weights for the 16 closure algorithms and considers their contrasts between land and ocean as well as more general local dependences. This feature enables representation of regime dependences of CUPs. Third, the ECP scheme includes numerous parameters and assumptions for *static control* that differ largely from those in the G3 scheme. These include entrainment or detrainment parameters for updrafts and downdrafts, assumptions for precipitation efficiencies, and varying ratios between downdraft and the updraft mass flux. Major assumptions and parameters for dynamic control, static control, and feedback in the ECP scheme are briefly summarized in supporting information Tables S1–S2. More details are presented below on the different algorithms for the five major types of closure assumptions. These algorithms differ in their physical basis and numerical implementation for computing the cloud base mass flux that is specifically required to close the heat/moisture budget equations.

The AS closure [*Arakawa and Schubert*, 1974] assumes an instantaneous equilibrium between large-scale forcing and subgrid convection by relaxing the cloud work function toward a climatological value. The cloud work function is an integral measure of the buoyancy force, resembling CAPE in principle but including the air parcel dilution from the environment [*Lee et al*., 2008]. Four algorithms are included, differing in the reference climatology for the cloud work function vertical profile as tabulated in *Lord et al*. [1982] from GATE observations and the Global Data Assimilation System (GDAS), and separated for levels above and below the convective cloud top.

The W closure [*Brown*, 1979; *Frank and Cohen*, 1987] assumes that net cloud base mass flux is determined by environmental upward vertical velocity averaged from the surrounding nine points at lower tropospheric levels. It includes four different algorithms by using environmental upward vertical velocity on the cloud base and the updraft originating level, and using the maximum and minimum upward vertical velocity below the cloud base.

The MC closure [*Krishnamurti et al*., 1983] assumes that total convective rainfall is proportional to the column integrated vertical advection of moisture. This variant can be redefined with four different algorithms by selecting maximum, minimum, averaged, or local randomly chosen values from the surrounding nine points. The cloud base mass flux is calculated by scaling the integrated vertical moisture advection with total convective rainfall.

The KF closure [*Kain and Fritsch*, 1993] assumes that convection acts to reduce the CAPE towards zero over a specific time scale. The TD closure is similar to the assumption in the *Grell* [1993] scheme, in which convection is determined by the increase of large-scale instability. Both the KF and TD closures contain two different subensembles by both defining the large-scale instability locally, and averaging it over the surrounding nine points.

The inclusion of tunable weighting and regional dependence for individual closures enable to optimize the ECP scheme by determining specific weights for different closures according to location, time, and more

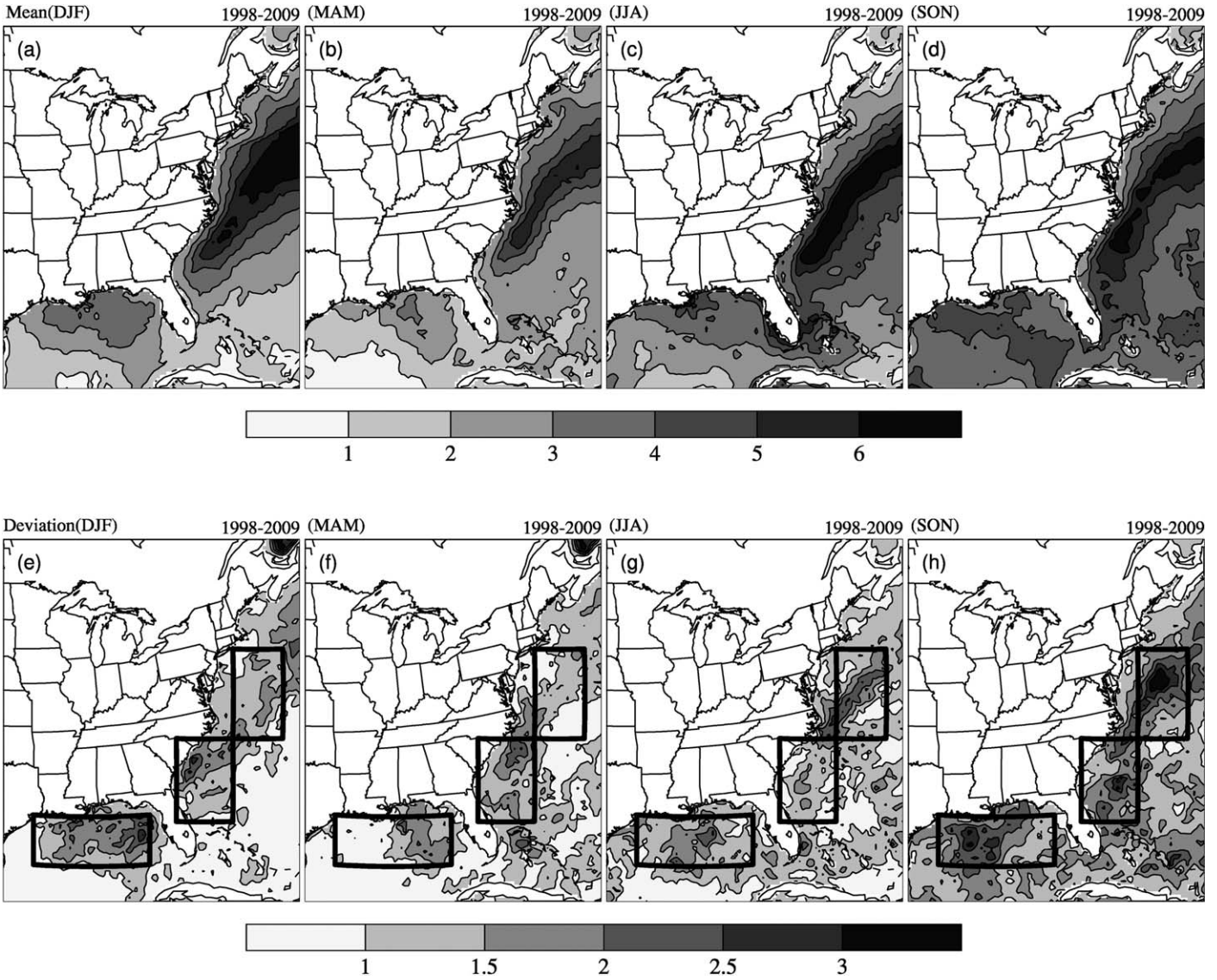

Figure 1. Geographic distribution of (top) TRMM precipitation (mm d^{-1}) seasonal climatology and (bottom) interannual standard deviation for winter (DJF), spring (MAM), summer (JJA), and fall (SON) averaged during 1998–2009. Outlined in the bottom figures are three key regions which are U.S. North Atlantic Coast (34°N–39°N, 75°W–67°W), U.S. South Atlantic Coast (28°N–34°N, 82°W–75°W), and the Gulf of Mexico (25°N–29°N, 95°W–84°W).

importantly, weather or climate regimes. To make this optimization, it is essential to understand the typical performance of individual closures in capturing precipitation characteristics. This study will comprehensively compare the sensitivity of U.S. coastal ocean rainfall simulation using these different closure algorithms built in the ECP scheme and will attempt to investigate whether the varying algorithms in each ensemble produce systematic errors or complement each other to generate relative small biases. The results will form the basis for selecting optimal closures for further improvement of the ECP scheme in the future.

4. Model Experiments

Figures 1a–1d show the observed seasonal mean precipitation distributions over the eastern U.S. coastal oceans within the CWRF computational domain during 1998–2009. There is a clear precipitation band along the U.S. Atlantic coastal oceans in all four seasons. The rainband is widest in winter (DJF, December–January–February) and narrowest in summer (JJA, June–July–August), but slightly discontinuous in autumn (SON, September–October–November) along the U.S. eastern coastlines and more widespread further east. The rainfall

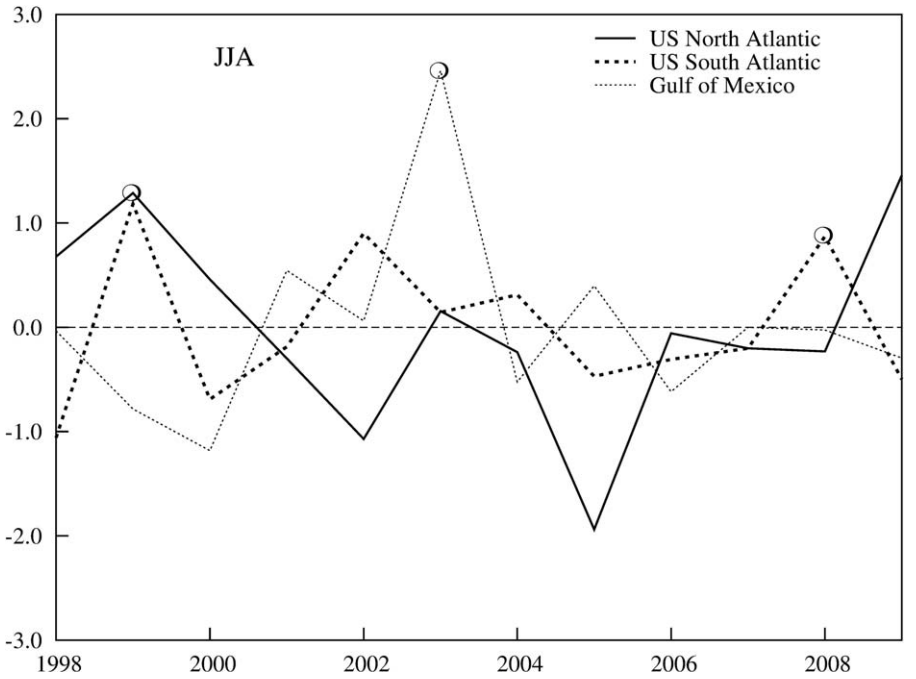

Figure 2. Summer (JJA) mean precipitation anomalies (mm d^{-1}) from the 1998–2009 climatology from the TRMM observations averaged over the three key coastal ocean regions outlined in Figure 1. Marked by circles are three cases with large precipitation anomalies, which are selected for further study.

intensity is weakest in spring (MAM, March–April–May) and strongest in summer. Figures 1e–1h present the interannual standard deviations of each season's mean precipitation from the mean climatology of 1998–2009. Large variances for all seasons are visible over the U.S. coastal oceans (hereafter, U.S. North Atlantic, U.S. South Atlantic, and Gulf of Mexico, as shown in the boxes). This study focuses on the summer, when the largest amount of precipitation is accompanied by the most intense convection along the U.S. coastal oceans [*Kuwano-Yoshida et al.*, 2010].

Figure 2 shows the average summer precipitation anomalies in each of the three key regions relative to the 1998–2009 climatology. Three cases with large summer precipitation anomalies were selected for further study: 2008 (U.S. South Atlantic), 2003 (Gulf of Mexico), and 1999 (U.S. North Atlantic). CWRF was used to conduct continuous integrations for each case. All included a 1 month spin-up, making the total period May–August. To systematically examine the cumulus closure effects over the coastal oceans, all CWRF experiments employed an identical physics configuration (Table 1) and used a default closure assumption over land that specified the moisture convergence plus cloud work function closure with an equal weight [*Liang et al.*, 2012]. Closure assumptions in the ECP scheme were varied only over the oceans. The sensitivity study first examined the differences between five ensemble closures that equally accounted for their respective members' contributions, and then separately compared each ensemble with its individual members for relative performance. Thus, each summer case contained 21 groups of sensitivity experiments, including 5 experiments with equal-weight ensemble averages of subensemble closures in each type and 16 experiments with each individual subensemble members. This comparison helps to systematically reveal the effects of cumulus closure assumptions with different conceptual underpinnings and varied parameters on summer heavy rainfall simulations over the U.S. coastal oceans.

5. Results

5.1. Effects of Ensemble Cumulus Closures

The ECP scheme includes the five major assumptions of cumulus closures (AS, W, MC, KF, and TD) summarized in section 3. These closures generally determine the convective cloud base mass flux by linking the convection with model-predicted variables such as cloud work function (or CAPE), moisture content, or

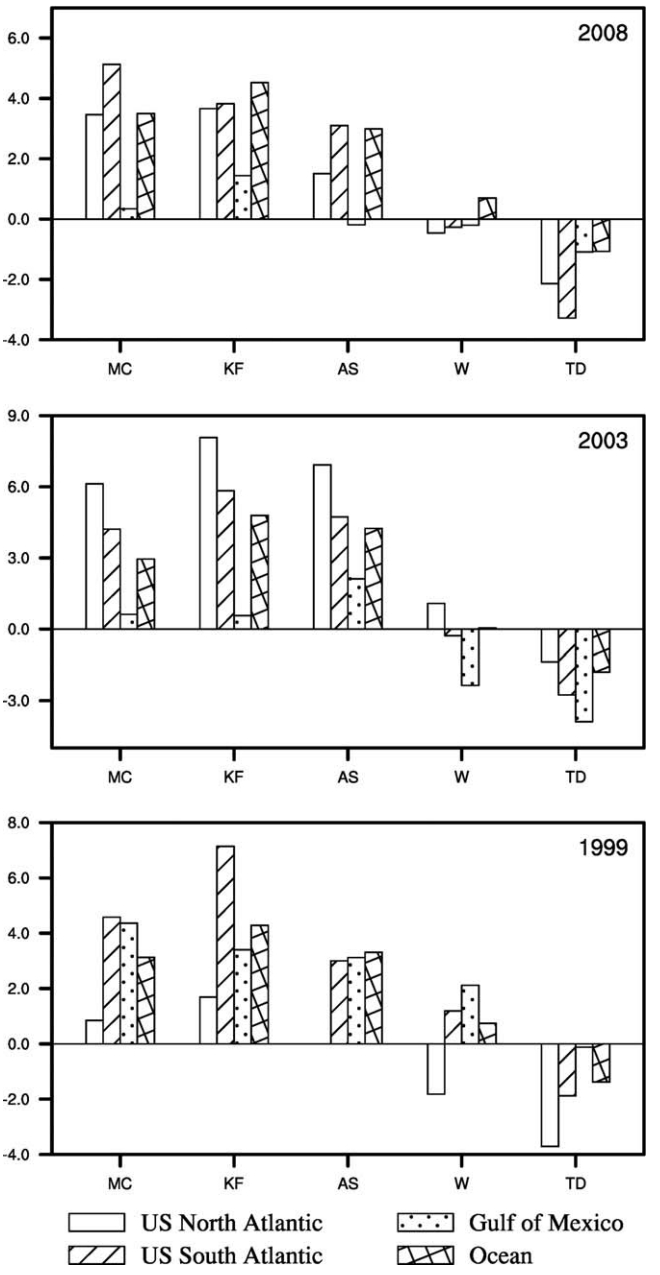

Figure 3. Three summer (2008, 2003, and 1999) mean precipitation biases (mm d^{-1}) averaged over the three coastal regions (U.S. North Atlantic Coast, U.S. South Atlantic Coast, and Gulf of Mexico) and the entire U.S. East and South coastal ocean simulated by CWRF using five ensemble closures (AS, W, MC, KF, and TD) as compared to the TRMM observations.

vertical velocity [*Grell and Dévényi*, 2002]. The study first investigated the predictive skills of these five different ensemble closures by setting equal weights for all algorithms in each type of assumptions.

5.1.1. Geographic Distribution of Summer Mean Precipitation

Figure 3 shows summer (2008, 2003, and 1999) mean precipitation biases simulated by CWRF using five cumulus ensemble closures (AS, W, MC, KF, and TD) averaged over each of the three key regions and the entire U.S. coastal oceans. For all three cases, the AS, MC, and KF closures largely overestimate rainfall amounts, while the TD closure systematically produces deficits. The W closure generates the smallest mean biases over these regions.

Figure 4 presents the geographic distributions of 2008 mean summer precipitation, the number of rainy days, and the average intensity conditioned on daily rainfall greater than 1 mm [*Yuan and Liang*, 2011] over the U.S. coastal oceans, as observed and simulated by CWRF using five ensemble closures. The result shows that the AS, MC, and KF closures all produce widespread excessive precipitation bands over the coastal oceans. The wet biases are caused by too many rainy days and unrealistically strong rain intensities. In contrast, the TD closure underestimates the rainfall amount and produces less rainy days than other closures, though still more than are observed. The W closure better captures the heavy rain band observed along the Gulf Stream but yields excessive rainfall amounts further east, mainly due to the overestimation of number of rainy days.

5.1.2. Precipitation Frequency and Intensity

Figure 5 shows the frequency distribution of 2008 summer pointwise daily precipitation over the U.S. coastal oceans, comparing the driving ERI reanalysis and the TRMM observations to the experimental simulations by CWRF using five ensemble cumulus closures. Precipitation rates are divided into 1 mm d^{-1} bins ranging from 0 to 55 mm d^{-1}, with rainfall higher than 55 mm d^{-1} accumulated into the last bin. The frequency calculation is based on the daily rainfall of all CWRF grids within the U.S. coastal oceans without any spatial or temporal averaging. ERI largely overestimates the frequency of light rain events with daily intensity less than 15 mm d^{-1} but produces hardly any heavy rain events exceeding 25 mm d^{-1}. The ECP schemes with five ensemble cumulus closures all produce much wider spectra than the ERI, though they

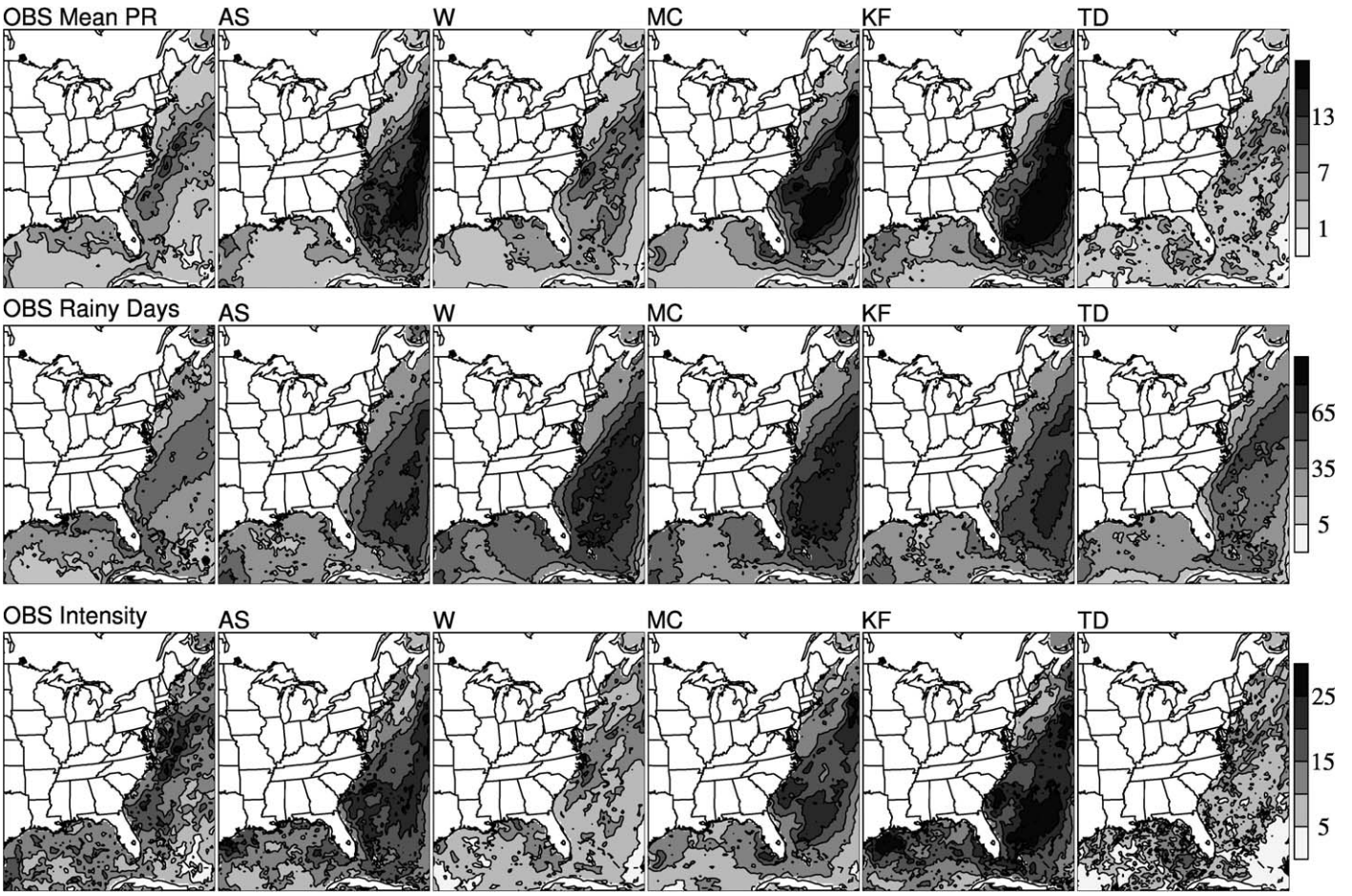

Figure 4. Geographic distributions of (top) 2008 summer mean precipitation (mm d^{-1}), (middle) the number of rainy days (for daily precipitation $>$ 1 mm d^{-1}), and (bottom) the mean rain intensity (mm d^{-1}) simulated by CWRF using five ensemble closures (AS, W, MC, KF, and TD) and the TRMM observations (OBS).

still fail to match reality. The AS, MC, and KF closures generally simulate rainy events ($>$5 mm d^{-1}) more frequent than TRMM, leading to their large wet biases. In contrast, the W and TD closures both underestimate the occurrence of heavy rain events, though they simulate different frequency distributions. For instance, the W closure underestimates the occurrence of rainfall greater than 20 mm d^{-1}, while the TD closure largely underestimates the contribution of rainfall greater than 5 mm d^{-1}. Clearly, the precipitation frequency distribution varies substantially with the choice of cumulus closures.

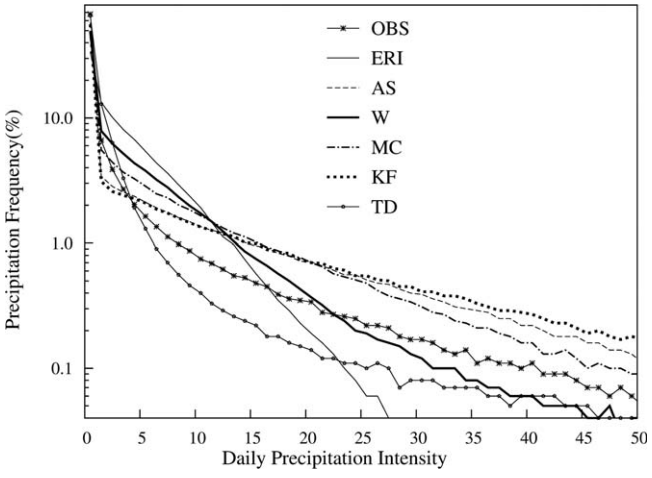

Figure 5. Frequency distributions (in logarithmic scales) of 2008 summer pointwise daily precipitation from each binned precipitation (1 mm d^{-1}) over the entire U.S. coastal oceans simulated by CWRF using five ensemble closures (AS, W, MC, KF, and TD), and compared to the ERI reanalysis and the TRMM observations.

5.1.3. Precipitation Diurnal Cycle

The observed ocean rainfall diurnal cycle is characterized by an early morning maximum [*Janowiak et al.*, 1994] over the open areas but with pronounced regional differences, such as the near-continental variations caused by the coastline effects and gravity wave forcing from the adjacent land [e.g., *Yang and Slingo*, 2001]. However, the true physical mechanisms responsible for

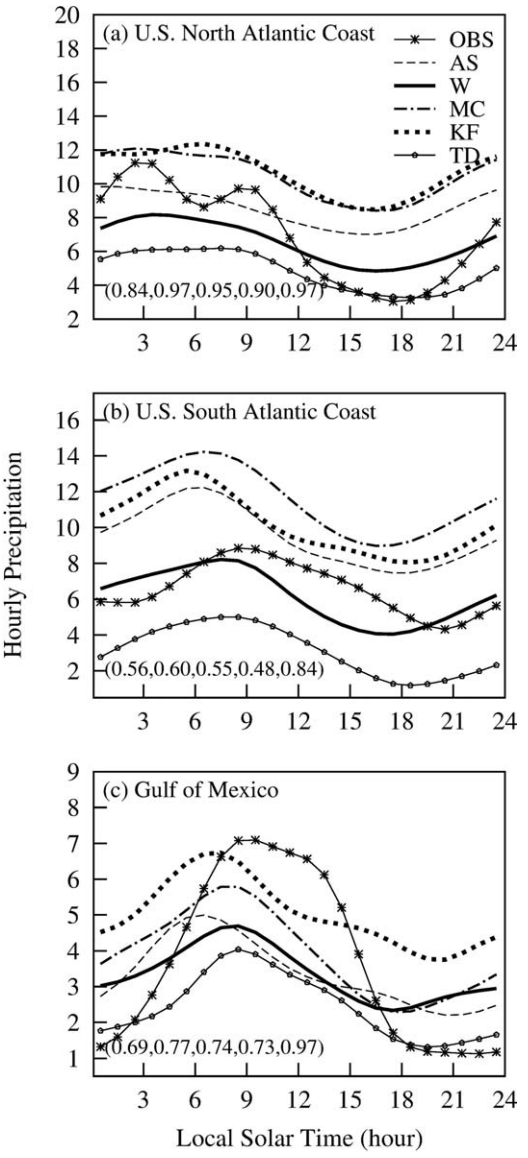

Figure 6. Mean diurnal variation (relative to local solar time) of precipitation (mm d^{-1}, correlation coefficients in the boxes), as observed by TRMM and as simulated by CWRF using five ensemble closures (AS, W, MC, KF, and TD) averaged over the three key regions: (a) U.S. North Atlantic Coast, (b) U.S. South Atlantic Coast, and (c) Gulf of Mexico.

this early morning rainfall peak are still not well known. *Nesbitt and Zipser* [2003] briefly summarize the possible causes into four general categories: (1) the differential radiative heating between convective and surrounding cloud-free regions; (2) the increased instability produced by nighttime radiative cooling near the cloud top; (3) the reduced cloud entrainment effects due to increased relative humidity at night; (4) the daily SST variations. These mechanisms suggest that the ocean rainfall diurnal cycle is modulated by the interaction between moist convection, cloud formation, radiation and surface processes [*Yang and Slingo*, 2001]. Thus, precipitation diurnal simulation provides an excellent test bed for evaluating these interactive physics processes [*Dai*, 2006].

All three summer cases show similar features in observed and simulated diurnal variations. Here we take the 2008 case as an example of these features. Figure 6 compares the TRMM observations of 2008 summer mean diurnal cycles of rainfall in the three key regions to those simulated by CWRF using the ECP scheme with five ensemble closures. Following *Liang et al*. [2004a], the 3-hourly precipitation data of TRMM and CWRF simulations are interpolated into hourly values by using spline fit method in order to examine the amplitude and phase of precipitation diurnal variations in higher temporal resolutions. The observed diurnal cycles vary in their phases and amplitudes along U.S. coastal oceans. There are clear early morning phase transitions, occurring at around 3 A.M. in the U.S. North Atlantic, 8 A.M. in the South Atlantic, and around 9–11 A.M. in the Gulf of Mexico. This phase behavior differs from previous findings in the tropical oceans where the mean rainfall peaks appear around 6–7 A.M. [*Nesbitt and Zipser*, 2003]. The delayed rainfall peaks over the latter two regions might be due to the effects of land convection migrating to the offshore areas, as has been suggested by earlier studies [*Zhou and Wang*, 2006].

The simulations show that the TD closure largely underestimates the rainfall peak amounts but captures the diurnal timing over the three regions better than other closures, with correlations of 0.97, 0.84, and 0.97 between observations and simulations. For the U.S. North Atlantic, all five closures capture the timing of the diurnal cycle well but have much weaker amplitudes than the observations. For the U.S. South Atlantic, the W closure captures the observed diurnal magnitudes but yields somewhat earlier peaks than TRMM, while the AS, MC, and KF closures substantially simulate the peaks 3 h early, and substantially overestimate their magnitudes. Over the Gulf of Mexico, the W and TD closures produce a precipitation maximum around 9 A.M. that is close to TRMM, but the other closures simulate much earlier rainfall peaks. These results suggest that the cumulus closures affect the regional variations of the U.S. coastal ocean rainfall diurnal cycle and indicate that the TD closure reproduces rainfall peaks at the right time over the eastern coastal regions. However, all these closures tend to underestimate diurnal amplitudes of precipitation over most coastal oceans. This is consistent with previous GCM simulations, which suggests a lack of appreciable SST diurnal forcing as one of the primary

causes [*Dai*, 1999]. Therefore, future sensitivity studies with UOM are required to examine how precipitation diurnal cycles are actually related to SST variations.

5.1.4. Overall Performance of the ECP Five Ensemble Closures

The above results identify several typical characteristics of the five ensemble cumulus closure assumptions. First, the AS, KF, and MC closures tend to overestimate the number of rainy days and the mean rain intensity, resulting in widespread large wet biases along the U.S. coastal oceans. Second, the W and TD closures reduce such biases but still contain significant deficiencies. For instance, the TD closure substantially overestimates the frequency of light rain less than 5 mm d^{-1}, leading to weaker rain intensities and total amount deficits, while the W closure simulates wet biases further east and overestimates the number of rainy days, largely because it overestimates the occurrence of daily precipitation of less than 20 mm d^{-1}. Third, the AS, MC, and KF closures overestimate diurnal magnitudes and generate earlier rainfall peaks than the observations, while the TD closure better captures the diurnal phase but underestimates the amplitude. Although the W closure produces a more realistic magnitude, falling between these two groups, it still has nontrivial phase errors. Therefore, none of these ensemble closure assumptions can fully represent all the observed precipitation characteristics. The inherent biases and distinct sensitivities among these ensemble cumulus closures suggest that U.S. coastal ocean precipitation simulations can be improved by refining the ECP ensemble closures.

5.2. Effects of Subensemble Closure Algorithms

To refine the ECP ensemble closures, this study examined the CWRF simulations using the ECP scheme with 16 separately selected subensemble closure algorithms and explored whether the use of different algorithms in each ensemble produces systematic errors or complement each other to generate smaller biases. The results may also provide guidance for future optimization of the ECP scheme, as appropriate weights can be derived for certain cumulus closures that can complementarily capture the observed signals [*Liang et al*., 2007].

5.2.1. Geographic Distribution of Summer Mean Precipitation

Figure 7 compares CWRF biases in summer precipitation when using each of the 16 subensemble closure algorithms, in the three key regions and over the U.S. coastal oceans. Biases are widely spread and some are systematic in certain ensemble closures. For instance, the AS and KF subensemble algorithms all overestimate the rainfall amounts, resulting in large wet biases in their ensembles, while all the TD algorithms systematically produce dry biases. The W and MC closure algorithms exhibit a wide distribution of biases, as the use of maximum vertical velocity at subcloud layer (W_3) and moisture convergence (MC_1) yield large wet biases, while that of the minimum vertical velocity at cloud base (W_1) and moisture convergence (MC_2) produce significant dry biases. Thus, the AS, KF, and TD ensemble closures generate errors that are systematic across all their subensemble algorithms, while the W and MC ensemble closures simulate reduced biases by cancellation of compensatory errors among their member algorithms. An important finding is that the algorithms based on the average vertical velocity at the cloud base or updraft originating level (W_2 or W_4), and moisture convergence (MC_3) consistently have smaller biases than other members.

The study evaluated the relative performance of three algorithms, W_2, MC_3, and TD_1, which are all based on the averaged large-scale forcings. The W_2 uses the average value of the environmental upward motion at the cloud base; the MC_3 uses the average value of the integrated vertical moisture advection; the TD_1 uses the average value of the cloud work function to derive the CAPE tendencies. Figure 8 compares the ERI reanalysis and the TRMM observations of geographic precipitation distributions in the three summer cases to those simulated by CWRF using above three subensemble closures. The ERI generally underestimates summer rainfall along the U.S. coastal oceans, consistent with the simulations of most GCMs [*Kuwano-Yoshida et al*., 2010]. The TD_1 produces significant deficits over coastal oceans, but the W_2 and MC_3 both reproduce the observed precipitation pattern and amount. The W_2 better captures the observed location of the major rainband along the Gulf Stream but simulates rainfall deficits, while the MC_3 improves the simulation of rainfall amounts but is spread across an unrealistically wide area.

Table 2 lists the pattern correlation coefficients and root-mean-square (rms) errors of summer (2008, 2003, and 1999) mean precipitation, number of rainy days, and precipitation intensity between the TRMM observations and the CWRF simulations using above three subensemble algorithms (W_2, MC_3, and TD_1) and their corresponding ensemble closures (W, MC, and TD). The W_2 and MC_3 better capture the geographic distribution of summer mean amounts, with comparable higher pattern correlations and smaller rms errors

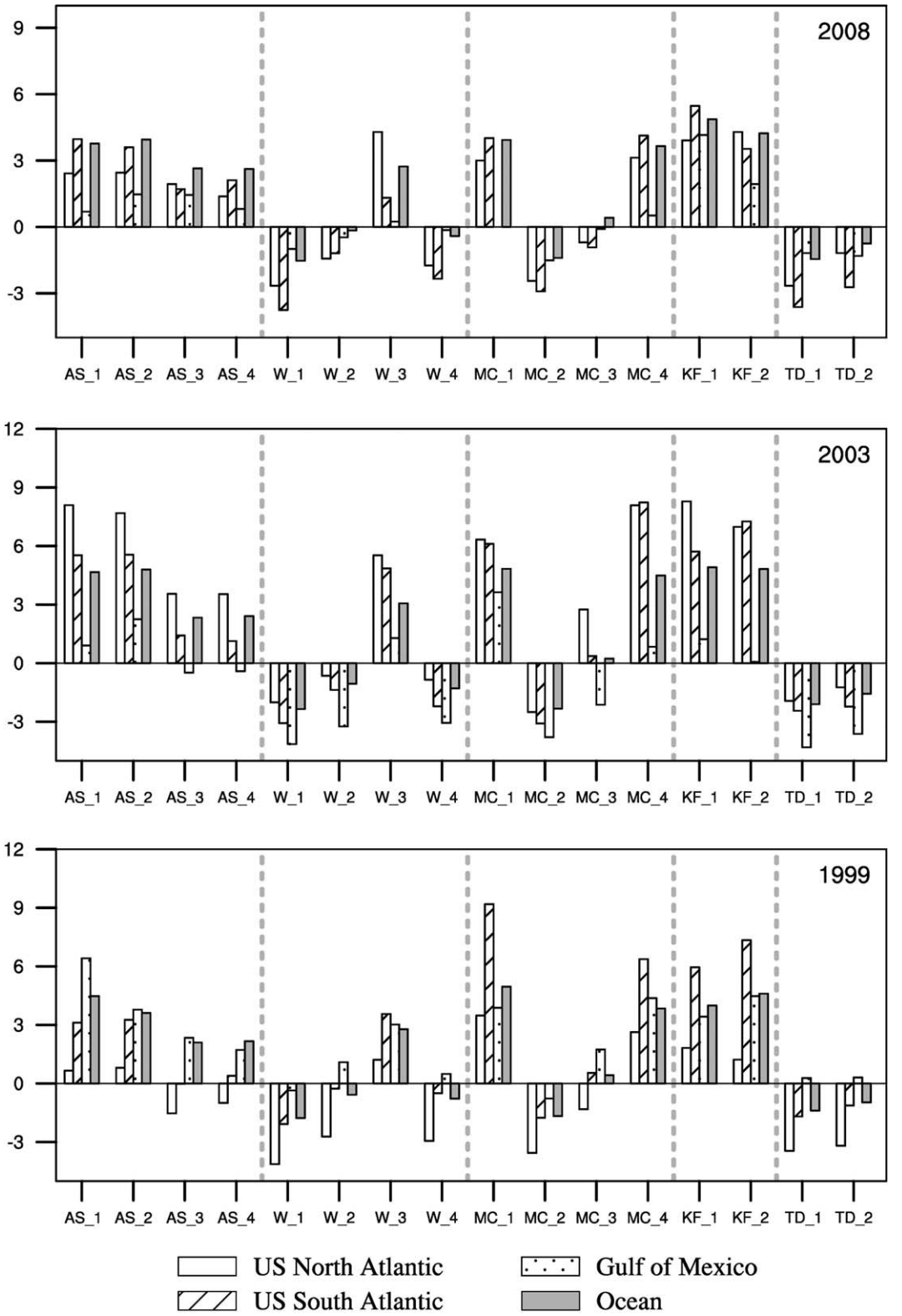

Figure 7. Mean precipitation biases (mm d^{-1}) in the three summer cases averaged over the key coastal regions and the entire U.S. coastal oceans simulated by CWRF using 16 subensemble closures, and compared to the TRMM observations.

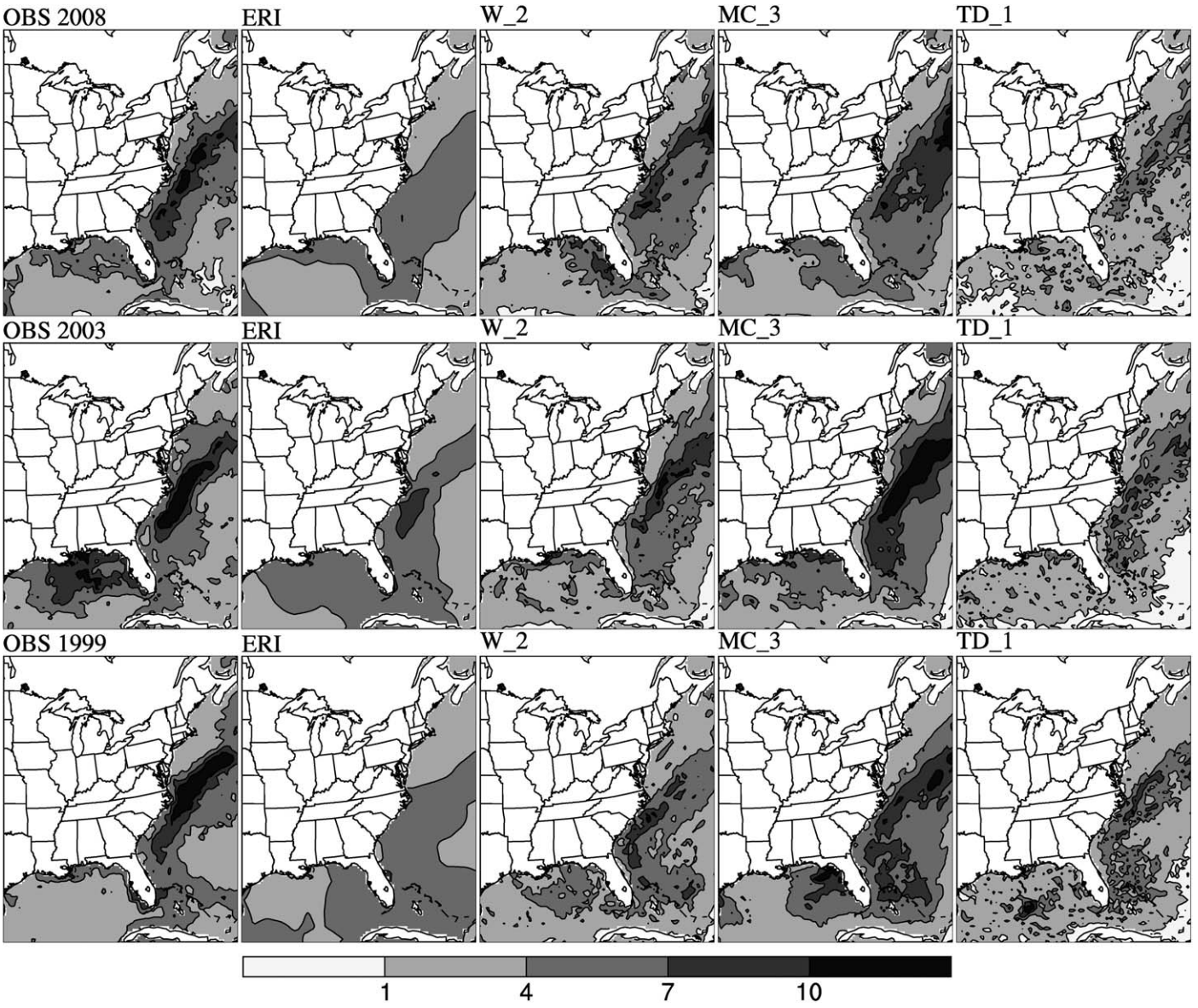

Figure 8. Geographic distributions of 2008, 2003, and 1999 summer mean precipitation (mm d^{-1}) simulated by CWRF using three subensemble closures (W_2, MC_3, and TD_1), and compared to the ERI reanalysis and the TRMM observations (OBS).

than the TD_1. Notably, the W_2 greatly reduces the overestimation of rainy days compared to the overall W ensemble, while the MC_3 improves rain intensity simulation from the entire MC ensemble. Thus, the other algorithms of these two ensemble closures are relatively less skilled and are better eliminated.

5.2.2. Precipitation Frequency and Intensity

Figure 9 compares the ERI reanalysis and TRMM observations of the frequency distributions of 2008 summer pointwise daily rainfall over the U.S. coastal oceans to those simulated by CWRF using the three subensemble closures (W_2, MC_3, and TD_1). All three CWRF simulations predict the frequency distribution better than the ERI, especially for heavy rain events greater than 25 mm d^{-1}. The TD_1 produces a similar distribution as its TD ensemble, with both generating insufficient occurrences of higher intensities. The W_2 and MC_3 both overestimate daily rainfall events weaker than 25 mm d^{-1} but slightly underestimate heavier rainfall events. The subensemble closure W_2 produces a frequency distribution of daily rainfall intensity that greatly resembles that generated by the W ensemble closure, particularly for the tail of extreme intensity. The subensemble closure MC_3 significantly reduces the overestimation of daily rainfall occurrences in the MC ensemble closure shown in Figure 5.

Table 2. Spatial Pattern Correlation Coefficient and rms Error Between Simulated by the ECP Scheme With Subensembles (W_2, TD_1, and MC_3) and Ensemble (W, TD, and MC) Closures and Observed Precipitation (Summer Mean, Number of Rainy Days, and Rain Intensity) Over the U.S. Coastal Oceans for Three Summer Experiments (2008, 2003, and 1999)[a]

		Summer Mean		Number of Rainy Days		Intensity	
Summer Cases	ECP Closures	Correlation	RMSE	Correlation	RMSE	Correlation	RMSE
2008	W_2	**0.69**	**1.79**	0.57	16	0.41	5.68
	W	0.63	2.15	0.47	23	0.40	5.26
	TD_1	0.62	2.34	**0.58**	**12**	0.19	7.02
	TD	0.59	2.19	0.47	12	0.15	6.52
	MC_3	**0.64**	**1.91**	0.48	22	**0.41**	**5.40**
	MC	0.53	5.51	0.41	23	0.40	5.50
2003	W_2	**0.62**	**2.34**	**0.56**	**14**	0.43	5.28
	W	0.54	2.52	0.48	22	0.41	4.88
	TD_1	0.55	3.04	0.51	17	0.33	5.65
	TD	0.52	2.93	0.43	19	0.28	5.84
	MC_3	**0.63**	**2.38**	0.51	21	**0.48**	**4.57**
	MC	0.52	4.90	0.46	22	0.43	5.00
1999	W_2	**0.53**	**2.86**	**0.51**	**14**	0.37	5.74
	W	0.49	2.61	0.51	19	0.41	5.09
	TD_1	0.50	2.61	0.46	13	0.22	6.24
	TD	0.54	2.52	0.43	11	0.33	6.17
	MC_3	**0.54**	**2.35**	0.50	18	**0.41**	**5.19**
	MC	0.38	4.82	0.45	18	0.32	6.72

[a]The bold numbers are the values that are closest to the observations.

Figure 10 shows the spatial frequency distributions of pointwise correlation coefficients and rms errors between the TRMM observations and the CWRF simulations using subensemble closures (W_2, MC_3, and TD_1) of daily rainfall variations for the three summer cases over the U.S. coastal oceans. Following *Liang et al*. [2012], the statistics are based on daily precipitation for all the grids over the U.S. coastal oceans in the CWRF domain. Frequency curves of the correlation coefficient (rms errors) shifted toward the right (left) indicate that the model is better able to capture the daily precipitation variation of temporal correspondence and magnitude. Clearly, the TD_1 is the worst overall, producing the lowest correlation and largest rms errors for all three cases, while W_2 and MC_3 show comparable performance in reproducing the observed temporal structure, except that the MC_3 is slightly superior with its correlation frequency shifting more to the right.

5.2.3. Precipitation Diurnal Cycle

Figure 11 compares the TRMM observations of the 2008 summer precipitation diurnal cycles to those simulated by CWRF using the three subensembles (W_2, MC_3, and TD_1) over the three key regions. The TD_1 has the typical characteristics of the TD ensemble, which captures the diurnal phase better than other closures but largely underestimates the magnitude. The MC_3 greatly reduces the overestimated magnitudes of the MC ensemble and produces a diurnal amplitude comparable with the W_2. However, both the W_2 and MC_3 produce weaker and earlier rainfall peaks than observations, suggesting that deep convection in these two assumptions still starts prematurely, lacking effective convective inhibition mechanisms [*Dai and Trenberth*, 2004]. In the ECP scheme, the convection trigger function is basically determined by maximum cap inversion (the depth between the cloud base and updraft originating level), which is 50 hPa over

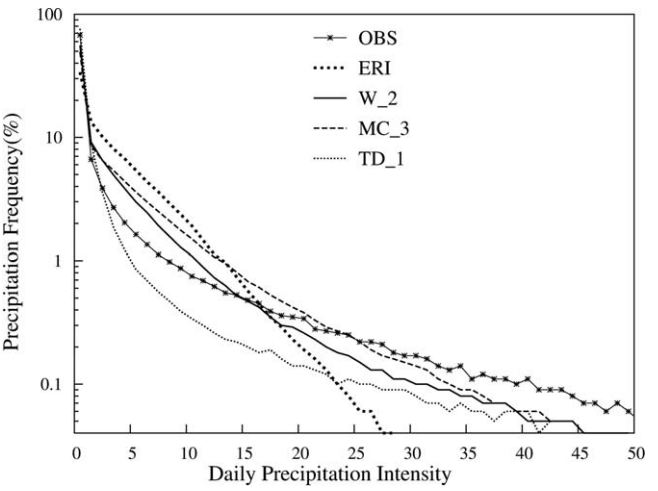

Figure 9. Frequency distributions (in logarithmic scales) of 2008 summer daily precipitation from each precipitation bin (1 mm d^{-1}) over the entire U.S. coastal oceans simulated by CWRF using three subensemble closures (W_2, TD_1, and MC_3), and compared to the ERI reanalysis and the TRMM observations.

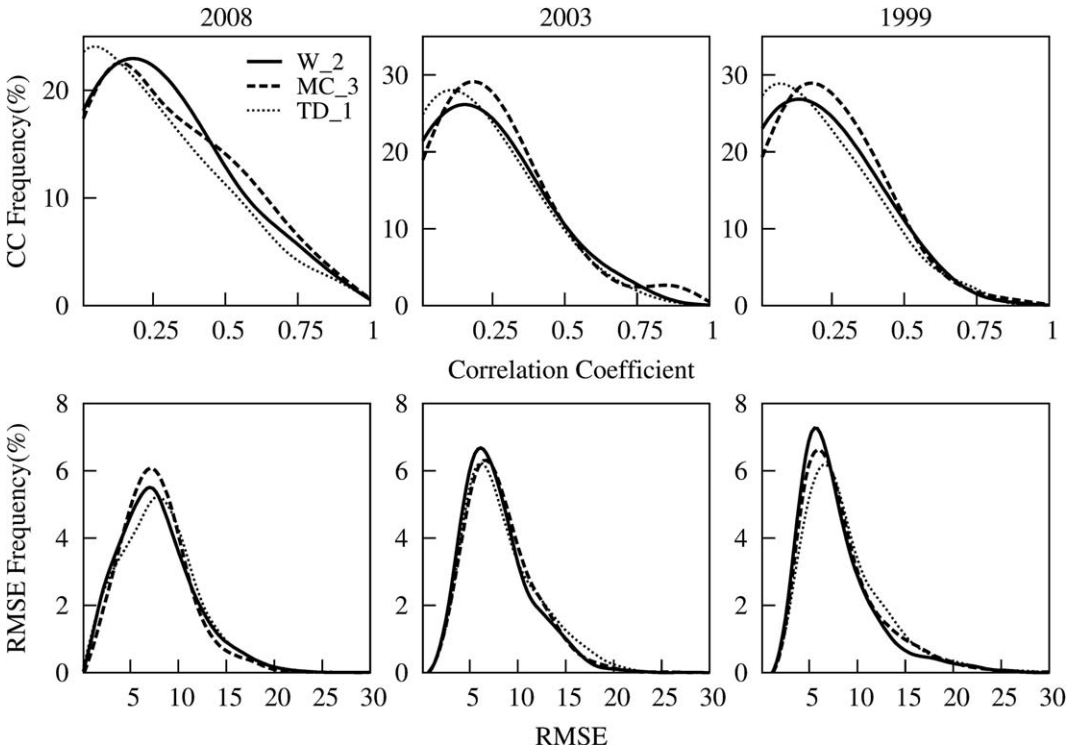

Figure 10. Spatial frequency distributions of pointwise correlation coefficients and rms errors (mm d^{-1}) of daily rainfall variations for the three summer cases (2008, 2003, and 1999) over the U.S. coastal oceans grids between the TRMM observations and CWRF simulations using three subensembles (W_2, MC_3, and TD_1).

oceans. The success of the TD_1 and TD ensemble in reproducing the diurnal phase may result from the inclusion of the CAPE (or cloud work function) increase rate as an additional constraint for convection initiation. This can be more generally implemented as a convective inhibiting trigger function [*Xie et al*., 2004].

6. Possible Causes for Different Cumulus Closure Effects

The study explored the spectra across 16 cumulus closures in simulating cloud base mass flux and convective-to-total precipitation ratio, thus demonstrating the widespread discrepancies in CWRF precipitation simulations caused by various closure assumptions. Two promising closures (W_2 and MC_3) were further studied to examine the correlations or differences of summer mean and daily variations among the CWRF simulated cloud base mass flux with CAPE, upward motion, and moisture convergence, as well as the convective and total precipitation over U.S. coastal oceans. The results will help explain possible causes for the complementary advantages of the W_2 and MC_3 in simulating summer mean precipitation pattern and intensity.

6.1. Cloud Base Mass Flux

The convective precipitation in CUP is parameterized by the precipitation efficiency with total condensate and cloud base mass flux, which is determined by different cumulus closure assumptions [*Arakawa*, 2004]. Thus, the cloud base mass flux directly affects the convective rainfall amount and results in different predictive skills among various closure assumptions. Figure 12 compares the frequency distributions of cloud base mass flux among 16 subensemble algorithms over the three key regions in June 2008. There are two distinct groups of cloud base mass flux distributions, which differ by more than 1 order of magnitude. The group with greater distribution magnitudes includes all the AS and KF closures, as well as the algorithms of maximum vertical velocity (W_3), and the maximum, average, and local random moisture convergence (MC_1, MC_3, and MC_4). Accordingly, all these closures systematically overestimate the precipitation amounts.

The group with 1 order smaller magnitude includes the algorithms of minimum vertical velocity (W_1) and moisture convergence (MC_2), the average vertical velocity at cloud base (W_2) and at updraft originating level (W_4), and two instability tendency assumptions (TD_1 and TD_2). These closures, however, differ in

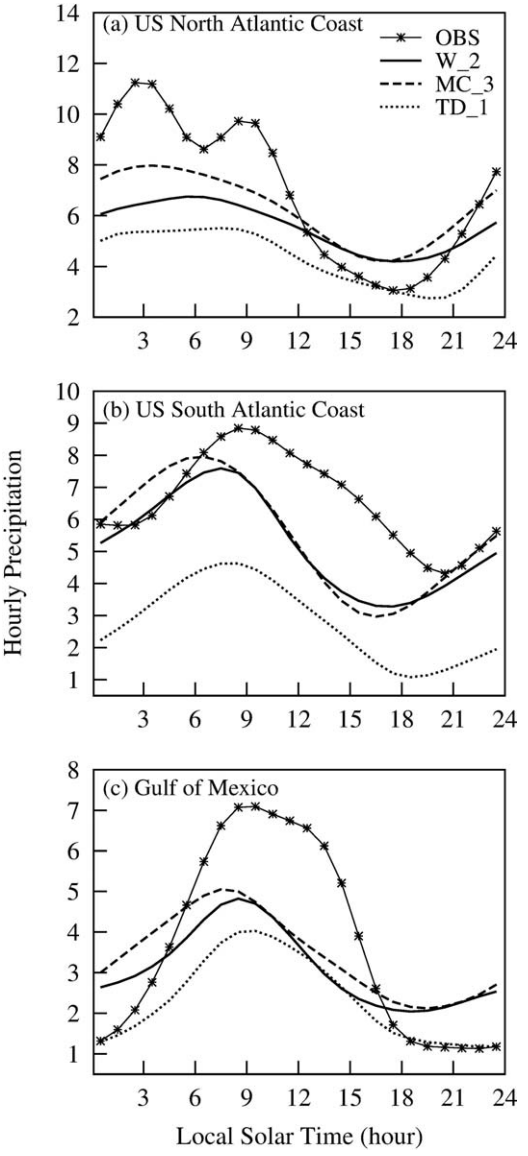

Figure 11. 2008 summer precipitation diurnal cycle (mm d^{-1}, relative to local solar time) simulated by CWRF using three subensemble closures (W_2, MC_3, and TD_1), and compared to the TRMM observations, all averaged over (a) the U.S. North Atlantic Coast, (b) the U.S. South Atlantic Coast, and (c) the Gulf of Mexico.

their frequency distributions of cloud base mass flux. The W_2 and W_4 both have much broader spectrums, while the others have a narrow band toward the lower end that may explain the larger rainfall deficits and drizzling problem in their frequency distributions.

6.2. Convective-to-Total Precipitation Ratio

It is important to examine the convective versus stratiform ratio, because these two types of precipitation have different vertical heating profiles, which significantly affect atmospheric large-scale circulation and climate simulations [*Houze*, 1997]. Most GCMs incorrectly partition precipitation between these two types, with excessive convective but insufficient stratiform precipitation [*Nesbitt and Zipser*, 2003; *Schumacher and Houze*, 2003; *Dai and Trenberth*, 2004; *Dai*, 2006]. The CUPs in these GCMs mostly adopt the CAPE-based closure assumptions, such as the *Zhang and McFarlane* [1995] scheme in which convection simply removes the CAPE over a given time scale. It has been suggested that this type of closure has deficiencies in parameterizing the convection intensity and its associated convective precipitation amounts [*Dai*, 2006; *Yang et al.*, 2013]. However, it is still unknown how different cumulus closures affect the convective-stratiform ratio over the U.S. coastal oceans and whether certain closures can produce a realistic partition.

Table 3 compares the TRMM 3A25 observations of the 2008 summer convective-to-total precipitation ratio to those simulated by CWRF using 16 subensemble closures over the three key and entire coastal ocean regions. The TRMM 3A25 data gives an average ratio of 64% over the entire U.S. coastal ocean region. The group of closures with a large magnitude of cloud base mass flux attributes total rainfall amounts predominantly to convection, with the ratio generally greater than 85%. Conversely, the closures with smaller cloud base mass flux, such as W_1 and MC_2, produce inadequate convective contributions of 18% or less. In this regard, it is encouraging that the W_2 (or W_4) closure well reproduces the observed ratio, albeit with a slight underestimation of total amounts. The MC_3, on the other hand, produces a much higher ratio (88%) than observed, but better captures the total precipitation amount (as previously described).

The summer mean pattern of cloud base mass flux highly correlates with that of convective rainfall in 2008 case, using the W_2 and MC_3 closure with the correlation coefficients of 0.95 and 0.88. This suggests that the model-simulated convective precipitation is strongly affected by distributions of cloud base mass flux. The MC_3 produces greater magnitude of cloud base mass flux than the W_2, and thus overestimates the convective rainfall amount, leading to an unrealistically large convective-to-total precipitation ratio.

6.3. Atmospheric Instability and Wind Vertical Structure

Examined below are the effects of cumulus closures on the distribution of cloud base mass flux, atmospheric instability (CAPE), large-scale upward motions, and vertical structure of wind convergence. This

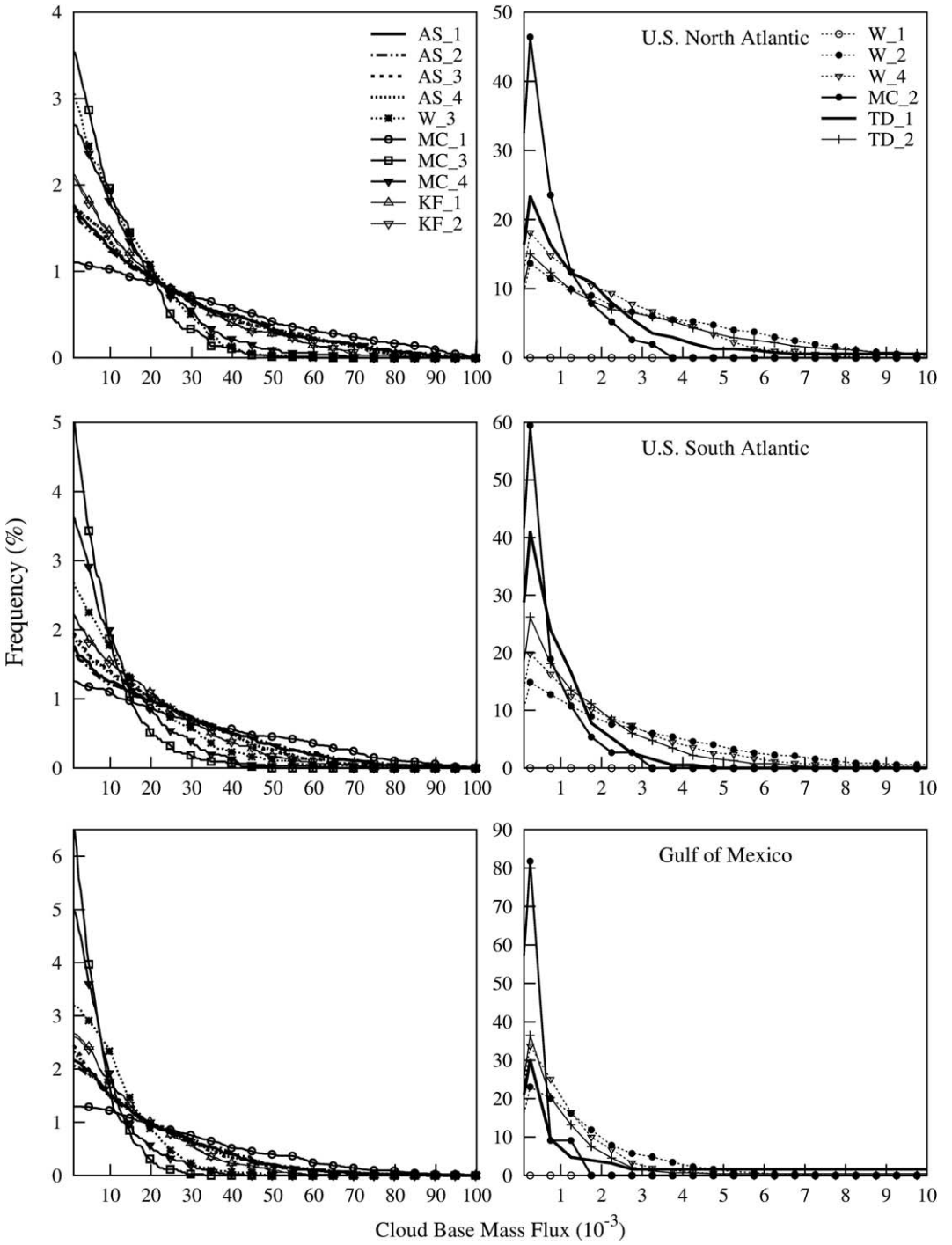

Figure 12. Spatial frequency distributions of 3-hourly pointwise cloud base mass flux (unit: kg m^{-2} s^{-2}) simulated by CWRF using 16 sub-ensemble closures over three U.S. coastal ocean regions in June 2008.

attempts to explain why the W_2 most realistically locates the major rainband along the Gulf Stream but simulates insufficient rainfall amounts, and the MC_3 increases intensity but overestimates rainband coverage.

Figure 13 presents the geographic distributions of 2008 summer mean observed SST, simulated cloud base mass flux, CAPE and convective precipitation, as well as upward motions at different latitudes (only show 500 hPa here) by CWRF using the three subensemble closures (W_2, MC_3, and TD_1). In each case, the

Table 3. Simulated Convective-to-Total Precipitation Ratio (%) Averaged Over the Three Key Coastal Ocean Regions for 2008 Summer by CWRF Using the ECP Scheme With 16 Subensemble Closures[a]

		AS				W				MC				KF		TD	
Regions	TRMM	1	2	3	4	1	2	3	4	1	2	3	4	1	2	1	2
U.S. North Atlantic	65	86	92	72	77	5	**61**	86	46	88	8	89	91	88	93	25	44
U.S. South Atlantic	57	89	93	81	81	11	**72**	95	64	97	15	91	95	88	98	29	50
Gulf of Mexico	62	98	95	94	94	10	**75**	98	63	98	16	92	99	95	99	30	56
Total	64	87	89	81	82	13	**69**	91	60	91	18	88	92	88	91	32	53

[a]The bold numbers are the values that are closest to the observations.

summer mean convective rainfall pattern highly resembles the distributions of cloud base mass flux and large-scale upward motion throughout the whole troposphere. The maximum rainbands are also associated with a high CAPE tongue that slants from the southwest to northeast, nearly parallel with the observed SST front, as suggested by *Minobe et al*. [2008] and *Kuwano-Yoshida et al*. [2010].

Substantial differences among the three subensemble closures help explain the predictive skills of CWRF using difference closure algorithms. The TD_1 produces much weaker cloud base mass flux and scattered upward motions along with relatively small CAPE, leading to insufficient amount of simulated convective precipitation. However, the MC_3 produces overly strong cloud base mass flux and a much wider band of CAPE tongue with stronger updrafts, explaining its relatively poor replication of precipitation patterns. Only the W_2 generates a narrow distribution of cloud base mass flux and CAPE tongue with updrafts closely following the more realistic convective precipitation band.

Figure 14 examines the daily correlations among the cloud base mass flux, CAPE, and convective precipitation, as simulated by CWRF using the three subensemble closures (W_2, MC_3, and TD_1). The correlation of daily variations between the CWRF simulated cloud base mass flux and the observed total precipitation is also given here for complete analyses. The correlations among the daily variations of cloud base mass flux, the CAPE, and the convective rainfall are the smallest and having the most scattering distribution in the TD_1 simulations. The W_2 and MC_3 both produce higher correlations for the daily variations among the cloud base mass flux, CAPE, and convective precipitation, except that the MC_3 shows relatively larger correlations between cloud base mass flux and observed total precipitation over the Gulf of Mexico. This higher correlation from the MC_3 also helps explain MC_3's superior skill in simulating daily precipitation variations over the entire U.S. coastal oceans as shown in Figure 10.

The study also examines the 2008 summer mean vertical structures of wind convergence averaged over the three key regions, as simulated by CWRF using the three subensemble closures (W_2, MC_3, and TD_1). The figure is not shown here. Over the U.S. Atlantic Coast, the MC_3 generates the largest wind convergence near the surface and divergence in the upper troposphere, consistent with the strongest upward motions and convective rainfall. In contrast, the TD_1 produces the weakest surface convergence and upper level divergence, and thus has much smaller upward motions and convective precipitation. This well explains the biases identified in the simulations of summer mean precipitation distributions using these subensemble closures. Therefore, cumulus closures significantly affect the distribution of cloud base mass flux and atmospheric instability, as well as upward motions associated with wind convergence, resulting in large differences in summer mean patterns and daily variations of convective precipitation.

7. Summary and Concluding Remarks

This study uses the ECP scheme incorporated in the mesoscale regional climate model CWRF to evaluate the effects of cumulus parameterization closure assumptions on summer precipitation variations over the U.S. coastal oceans. The ECP scheme includes five major groups of closure assumptions, with 16 different algorithms in together, to determine cloud base mass flux, and it allows us to examine the isolated performance of individual closure algorithms over land and oceans separately while other components such as trigger function and cloud model remain unchanged.

The TRMM observations show that large interannual precipitation variability exists over the U.S. coastal oceans, especially in the north and south portions of the U.S. Atlantic and the Gulf of Mexico. A series of

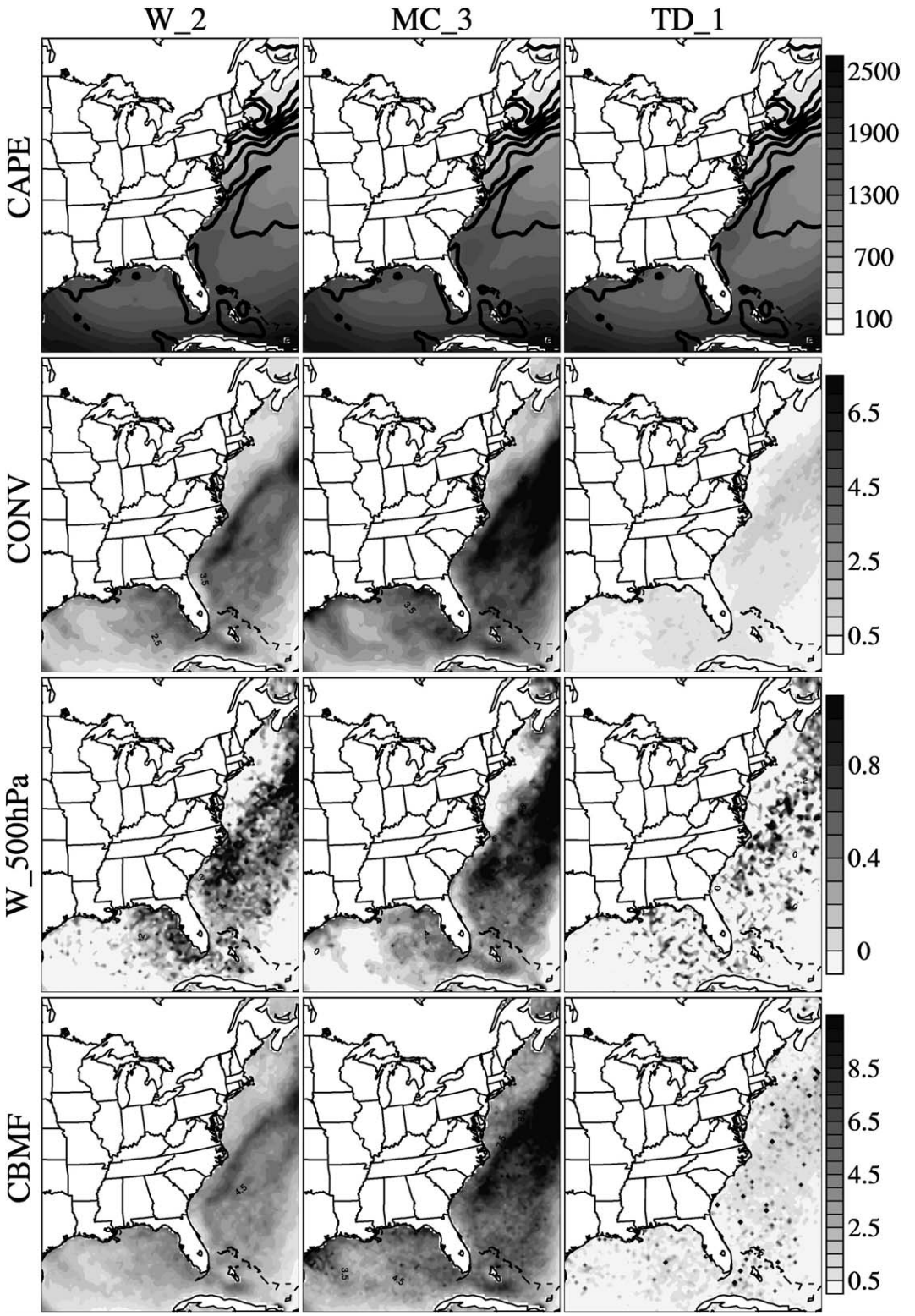

Figure 13. Geographic distributions of (top) 2008 summer mean observed SST (solid lines with interval of 1°C), CWRF simulated CAPE (shaded, J kg^{-1}), (middle first row) convective precipitation (CONV, mm d^{-1}), and (middle second row) mean vertical velocity (W_500 hPa, 10^{-2} m s^{-1}) at 500 hPa, as well as (bottom) the cloud base mass flux (CBMF, 10^{-3} kg m^{-2} s^{-2}) as simulated using three subensemble closures (W_2, MC_3, and TD_1).

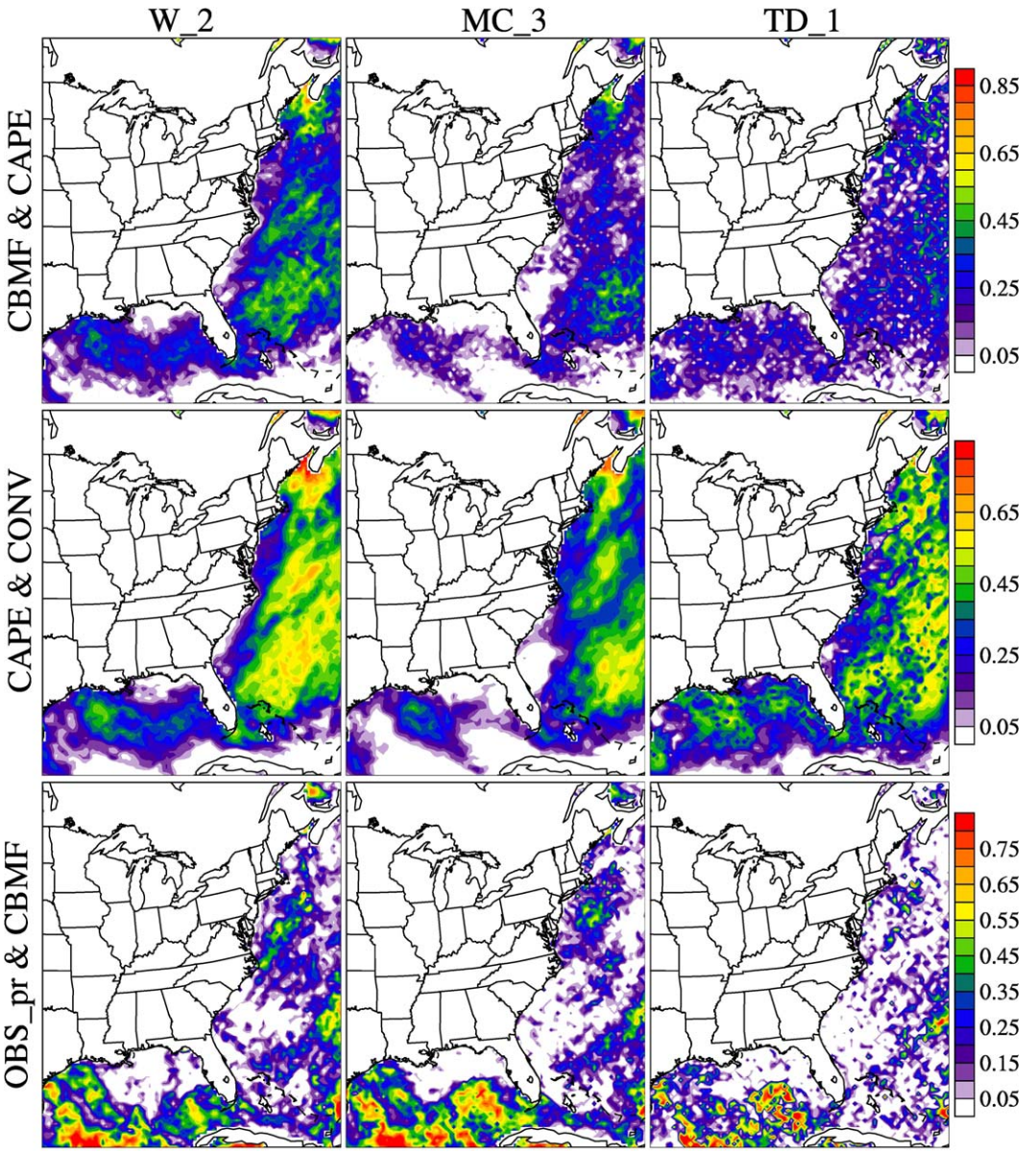

Figure 14. 2008 summer geographic distributions of (top) daily correlations between CWRF simulated cloud base mass flux and CAPE (CBMF & CAPE), (middle) between CWRF simulated CAPE and convective precipitation (CAPE & CONV), and (bottom) between observed precipitation and CWRF simulated cloud base mass flux (OBS_Pr & CBMF) using the ECP scheme with three subensemble closures (W_2, MC_3, and TD_1).

CWRF integrations using the ECP scheme with five ensemble closures (AS, W, MC, KF, and TD) were performed for three summers (2008, 2003, and 1999) when abnormally heavy rainfall occurred over the above key areas. The results show that closure assumptions largely affect the CWRF simulations of U.S. coastal ocean summer precipitation. The AS, KF, and MC closures produce widespread wet biases along the entire U.S. coastal oceans due to overestimation of the number of rainy days and rain intensity. The TD closure better captures the occurrence of rainy days than other closures, but it overestimates the frequency of light rain events and thus yields large deficits in rainfall amount. The W closure better captures the rainband along the U.S. Atlantic Coast but overestimates the rainy days and total amounts further east. Although it better simulates the diurnal phase, the TD closure systematically underestimates rainfall amounts. Thus, none of these ensemble closure assumptions can fully represent all the observed precipitation characteristics.

Further experiments using the ECP scheme with 16 subensemble closure algorithms show that different algorithms using the same physical concepts can have pronounced impacts on ocean precipitation simulation. The algorithms based on the average vertical velocity at cloud base (W_2) and moisture convergence

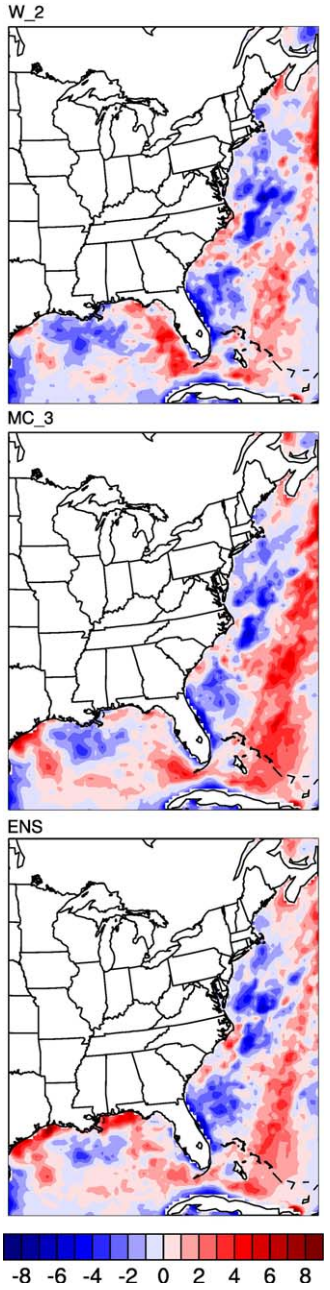

Figure 15. Geographic distributions of 2008 summer mean precipitation biases (mm d^{-1}) between observations and three CWRF simulations using the W_2, the MC_3 closures, and their optimal ensemble (ENS) closure (specific weights of 2.0 for W_2 and 0.5 for MC_3).

(MC_3) complementarily reproduce the observed precipitation pattern and amount, and capture the frequency of heavy rainfall events better than other closures. For the diurnal cycle, the instability tendency closures (TD_1 or TD) better capture the rainfall diurnal phase but with larger deficits in peak values. This suggests that cloud base vertical velocity and moisture convergence may be the primary factors controlling precipitation seasonal mean and daily variation, while the instability tendency may play a more critical role in regulating the diurnal phase. Our findings are supported by previous studies that suggest the large-scale ascent as an important dynamical control of precipitation occurrence in the tropics [*Barlow et al*., 1998] and the moisture flux convergence as a significant contributor to U.S. daily precipitation variations [*Becker et al*., 2009].

The large disparities in model biases among these cumulus closures directly arise from their formulation differences in computing the cloud base mass flux. The ECP closures can be divided into two major groups that differ in cloud base mass flux magnitude. The first group, which has 1 order larger magnitude, encompasses all the closure algorithms that produce excessive precipitation, while second group, which has smaller cloud base mass flux, systematically generates precipitation deficits. Note that several critical variants in closure algorithms are highly empirical with strong scale dependence. For example, the AS closure assumes a specific time interval (1200 s) to consume the CAPE departure from a prescribed climatological value; the KF closure assumes a relaxation time scale (2400 s) to remove the total CAPE; and the TD closure employs a shorter time scale (240 s) to deplete the increase of CAPE. Although precipitation biases may be reduced to a certain extent through reasonable adjustment of the time scale [*Yang et al*., 2012], our sensitivity experiments show that their effects are relatively small compared to the contrasts between the closures discussed above.

Cumulus closures affect the coastal ocean precipitation simulation mainly through their impacts on the distributions of cloud base mass flux and atmospheric instability, as well as large-scale updrafts associated with wind convergence. In particular, the W_2 simulates a narrow band of cloud base mass flux distribution, upward motion, CAPE tongue, and convective precipitation, but the MC_3 produces a widespread distribution of cloud base mass flux, stronger upward motion, and convective precipitation associated with a wide CAPE tongue. This explains why the W_2 more realistically captures the spatial distribution of a major rainband but insufficiently captures rainfall amount, while the MC_3 improves the rainfall amount but has an unrealistically widespread pattern.

A set of preliminary CWRF experiments were conducted for the summer of 2008 using an ensemble of the two promising closures (W_2 and MC_3) with different weights in the ECP. Figure 15 presents the geographic distributions of 2008 summer mean precipitation biases of CWRF simulations using the W_2 and MC_3 closures, and their ensemble (ENS) with respective constant weights of 2.0 and 0.5. The weights adjust the model-predicted cloud base mass flux, which is essential for the simulation of convective precipitation amount and location. The use of this ensemble clearly reduces the large wet bias produced by the MC_3 along the U.S. east coast oceans and mitigates the dry bias near the northern coastlines in the W_2. This improvement suggests that the appropriately weighted closure ensemble is superior to individual closures for summer mean precipitation simulations over U.S. coastal oceans. In the future, we will consider dynamic selections and weights of optimal closures based on prevailing climate regime characteristics.

Despite the fairly realistic pattern of summer mean rainfall amounts, W_2 and MC_3 still overpredict the number of rainy days. This indicates that the moist convection in the ECP scheme is triggered prematurely and occurs too often. This deficiency is also evident in the diurnal cycle simulation, as the W_2 and MC_3 tend to produce earlier rainfall peaks than are observed. On the other hand, the TD_1 generates reduced rainy days and better reproduces the diurnal phase. Thus, it is likely to inhibit the convection by adding the instability tendency as an additional trigger function in the ECP scheme to improve the frequency distribution and diurnal cycle.

It should be noted that the difficulties in accurately simulating the ocean precipitation diurnal cycle could also be caused by deficiencies in other related physical processes, such as SST, the planetary boundary layer, and cloud microphysics [*Dai and Trenberth*, 2004]. Thus, the improvement of ocean rainfall diurnal simulation requires a better understanding and representation of these processes. Additionally, the model verification is influenced by uncertainty in the observational data. For example, the latest TRMM 3B42 version 7 has improved rainfall intensity estimates with substantial differences from the previous release, leading to some nontrivial modifications of the interpretation of the model "biases." Further deviations are expected as the accuracy of TRMM data is still uncertain. Nevertheless, the ECP scheme provides an unprecedented opportunity to identify the typical behaviors of these cumulus closures. The objective diagnostic procedure established in this study can effectively guide future refinements of the ECP scheme through ensemble closure optimization to enhance precipitation predictive skills against more accurate observations as they emerge.

Acknowledgments
We thank Georg Grell for developing and providing guidance on the application of the G3 scheme which forms the basis of the ECP scheme in the CWRF. We are also appreciative of Tiejun Ling and Min Xu for helping with CWRF post processing job scripts. We thank Jennifer Kennedy for thorough English editing. This research was supported by China Postdoctoral Science Foundation (2014M561437), Science and Technology Commission of Shanghai Municipality (13231203804), NOAA (EPP) COM Howard (631017) and the USDA NIFA 2015-34263-24070 (subawards to the University of Maryland, G-89701-2). The model simulations were conducted at the DOE/NERSC, NOAA/ESRL, UIUC/NCSA and ECNU/Shuguang supercomputing facilities. The views expressed are those of the authors and do not necessarily reflect those of the sponsoring agencies.

References

Arakawa, A. (2004), The cumulus parameterization problem: Past, present, and future, *J. Clim.*, *17*, 2493–2525.
Arakawa, A., and W. H. Schubert (1974), Interaction of a cumulus cloud ensemble with the large-scale environment, Part I, *J. Atmos. Sci.*, *31*, 674–701.
Barlow, M., S. Nigam, and E. H. Berbery (1998), Evolution of the North American Monsoon System, *J. Clim.*, *11*, 2238–2257.
Bechtold, P., J.-P. Chaboureau, A. Beljaars, A. K. Betts, M. Köhler, M. Miller, and J.-L. Redelsperger (2004), The simulation of the diurnal cycle of convective precipitation over land in a global model, *Q. J. R. Meteorol. Soc.*, *130*, 3119–3137.
Becker, E. J., E. H. Berbery, and R. W. Higgins (2009), Understanding the characteristics of daily precipitation over the United States Using the North American Regional Reanalysis, *J. Clim.*, *22*, 6268–6286.
Brown, J. M. (1979), Mesoscale unsaturated downdrafts driven by rainfall evaporation: A numerical study, *J. Atmos. Sci.*, *36*, 313–338.
Choi, H. I., and X.-Z. Liang (2010), Improved terrestrial hydrologic representation in mesoscale land surface models, *J. Hydrometeorol.*, *11*, 797–809.
Choi, H. I., X.-Z. Liang, and P. Kumar (2013), A conjunctive surface-subsurface flow representation for mesoscale land surface models, *J. Hydrometeorol.*, *14*, 1421–1442.
Chou, M.-D., and M. J. Suarez (1999), A solar radiation parameterization for atmospheric studies. [Last revision on March 2002], in *Technical Report Series on Global Modeling and Data Assimilation*, vol. *15*, edited by M. J. Suarez, 42 pp., NASA/TM-1999-104606, Goddard Space Flight Cent., Greenbelt, Md.
Dai, A. (1999), Recent changes in the diurnal cycle of precipitation over the United States, *Geophys. Res. Lett.*, *26*, 341–344.
Dai, A. (2006), Precipitation characteristics in eighteen coupled climate models, *J. Clim.*, *19*, 4605–4630.
Dai, A., and K. E. Trenberth (2004), The diurnal cycle and its depiction in the Community Climate System Model, *J. Clim.*, *17*, 930–951.
Dee, D. P., et al. (2011), The ERA-Interim reanalysis: Configuration and performance of the data assimilation system, *Q. J. R. Meteorol. Soc.*, *137*, 553–597.
Donner, L. J. (1993), A cumulus parameterization including mass fluxes, vertical momentum dynamics, and mesoscale effects, *J. Atmos. Sci.*, *50*, 889–906.
Fletcher, J. K., and C. S. Bretherton (2010), Evaluating boundary layer-based mass flux closures using cloud-resolving model simulations of deep convection, *J. Atmos. Sci.*, *67*, 2212–2225.
Frank, W. M., and C. Cohen (1987), Simulation of tropical convective systems. Part I: A cumulus parameterization, *J. Atmos. Sci.*, *44*, 3787–3799.
Gochis, D. J., W. J. Shuttleworth, and Z.-L. Yang (2002), Sensitivity of the modeled North American Monsoon regional climate to convective parameterization, *Mon. Weather Rev.*, *130*, 1282–1298.
Grell, G. A. (1993), Prognostic evaluation of assumptions used by cumulus parameterizations, *Mon. Weather Rev.*, *121*, 764–787.
Grell, G. A., and D. Dévényi (2002), A generalized approach to parameterizing convection combining ensemble and data assimilation techniques, *Geophys. Res. Lett.*, *29*(14), doi:10.1029/2002GL015311.
Houze, R. A. (1997), Stratiform precipitation in regions of convection: A meteorological paradox?, *Bull. Am. Meteorol. Soc.*, *78*, 2179–2196.
Iguchi, T., T. Kozu, R. Meneghine, J. Awaka, and K. Okamoto (2000), Rain-profiling algorithm for the TRMM precipitation radar, *J. Appl. Meteorol.*, *39*, 2038–2052.
Janowiak, J. E., P. A. Arkin, and M. Morrissey (1994), An examination of the diurnal cycle in oceanic tropical rainfall using satellite and in situ data, *Mon. Weather Rev.*, *122*, 2296–2311.
Kain, J. S., and J. M. Fritsch (1993), Convective parameterization for mesoscale models: The Kain-Fritcsh scheme, The Representation of Cumulus Convection in Numerical Models, Meteorological Monographs, 24.
Kahn, R. A., B. J. Gaitley, J. V. Martonchik, D. J. Diner, K. A. Crean, and B. Holben (2005), Multiangle Imaging Spectroradiometer (MISR) global aerosol optical depth validation based on 2 years of coincident Aerosol Robotic Network (AERONET) observations, *J. Geophys. Res.*, *110*, D10S04, doi:10.1029/2004JD004706.
Krishnamurti, T. N., S. Low-Nam, and R. Pasch (1983), Cumulus parameterization and rainfall rates II, *Mon. Weather Rev.*, *111*, 815–828.
Kuo, H. L. (1974), Further studies of the parameterization of the influence of cumulus convection on large-scale flow, *J. Atmos. Sci.*, *31*, 1232–1240.

Kuwano-Yoshida, A., S. Minobe, and S.-P. Xie (2010), Precipitation response to the gulf stream in an atmospheric GCM, *J. Clim.*, *23*, 3676–3698.
Li, G., and S. Xie (2014), Tropical biases in CMIP5 multi-model ensemble: The excessive equatorial Pacific cold tongue and double ITCZ problems, *J. Clim.*, doi:10.1175/JCLI-D-13-00337.1.
Liang, X.-Z., and F. Zhang (2013), The Cloud-Aerosol-Radiation (CAR) ensemble modeling system, *Atmos. Chem. Phys.*, *13*, 8335–8364.
Liang, X.-Z., L. Li, A. Dai, and K. E. Kunkel (2004a), Regional climate model simulation of summer precipitation diurnal cycle over the United States, *Geophys. Res. Lett.*, *31*, L24208, doi:10.1029/2004GL021054.
Liang, X.-Z., L. Li, K. E. Kunkel, M. Ting, and J. X. L. Wang (2004b), Regional climate model simulation of U.S. precipitation during 1982-2002. Part 1: Annual cycle, *J. Clim.*, *17*, 3510–3528.
Liang, X.-Z., M. Xu, K. E. Kunkel, G. A. Grell, and J. S. Kain (2007), Regional climate model simulation of U.S.–Mexico summer precipitation using the optimal ensemble of two cumulus parameterizations, *J. Clim.*, *20*, 5201–5207, doi:10.1175/JCLI4306.1.
Liang, X.-Z., et al. (2012), Regional Climate-Weather Research and Forecasting Model (CWRF), *Bull. Am. Meteorol. Soc.*, *93*, 1363–1387.
Lin, J.-L. (2007), The double-ITCZ problem in IPCC AR4 coupled GCMs: Ocean–atmosphere feedback analysis, *J. Clim.*, *20*, 4497–4525.
Ling, T., M. Xu, X.-Z. Liang, J. X. L. Wang, and Y. Noh (2015) A multilevel ocean mixed layer model resolving the diurnal cycle: Development and validation, *J. Adv. Model. Earth Syst.*, *7*, 1680–1692, doi:10.1002/2015MS000476.
Lord, S. J., W. C. Chao, and A. Arakawa (1982), Interaction of a cumulus cloud ensemble with the large-scale environment. Part IV: The Discrete Model, *J. Atmos. Sci.*, *39*, 104–113.
Maloney, E. D., and D. L. Hartmann (2001), The sensitivity of intraseasonal variability in the NCAR CCM3 to changes in convective parameterization, *J. Clim.*, *14*, 2015–2034.
Minobe, S., A. Kuwano-Yoshida, N. Komori, S.-P. Xie, and R. J. Small (2008), Influence of the Gulf Stream on the troposphere, *Nature*, *452*, 206–209.
Molinari, J., and M. Dudek (1992), Parameterization of convective precipitation in mesoscale numerical models: A Critical Review, *Mon. Weather Rev.*, *120*, 326–344.
Nesbitt, S. W., and E. J. Zipser (2003), The diurnal cycle of rainfall and convective intensity according to three years of TRMM measurements, *J. Clim.*, *16*, 1456–1475.
Park, S., and C. S. Bretherton (2009), The University of Washington shallow convection and moist turbulence schemes and their impact on climate simulations with the Community Atmosphere Model, *J. Clim.*, *22*, 3449–3469.
Qiao, F., and X.-Z. Liang (2015), Effects of cumulus parameterizations on predictions of summer flood in the Central United States, *Clim. Dyn.*, *45*, 727–744.
Reynolds, R. W., N. A. Rayner, T. M. Smith, D. C. Stokes, and W. Wang (2002), An improved in situ and satellite SST analysis for climate, *J. Clim.*, *15*, 1609–1625.
Rontu, L. (2006), A study on parameterization of orography-related momentum fluxes in a synoptic-scale NWP model, *Tellus, Ser. A*, *58*, 69–81.
Sato, T., H. Miura, M. Satoh, Y. N. Takayabu, and Y. Wang (2009), Diurnal cycle of precipitation in the tropics simulated in a global cloud-resolving model, *J. Clim.*, *22*, 4809–4826.
Schumacher, C., and R. A. Houze Jr. (2003), Stratiform rain in the tropics as seen by the TRMM precipitation radar, *J. Clim.*, *16*, 1739–1756.
Skamarock, W. C., J. B. Klemp, J. Dudhia, D. O. Gill, D. M. Barker, M. G. Duda, X.-Y. Huang, W. Wang, and J. G. Powers (2008), A Description of the Advanced Research WRF Version 3, Mesoscale and Microscale Meteorology Division, NCAR technical note NCAR/TN475 1 STR, 113 pp., Nat. Cent. Atmos. Res., Boulder, Colo.
Sun, Y., S. Solomon, A. Dai, and R. W. Portmann (2006), How often does it rain?, *J. Clim.*, *19*, 916–934.
Sutton, R. T., and D. L. R. Hodson (2007), Climate response to basin-scale warming and cooling of the North Atlantic Ocean, *J. Clim.*, *20*, 891–907.
Tao, W.-K, et al. (2003), Microphysics, radiation and surface processes in the Goddard Cumulus Ensemble (GCE) model, *Meteorol. Atmos. Phys.*, *82*, 97–137.
Wilcox, E. M., and L. J. Donner (2007), The frequency of extreme rain events in satellite rain-rate estimates and an Atmospheric General Circulation Model, *J. Clim.*, *20*, 53–69.
Wu, X., X.-Z. Liang, and G. J. Zhang (2003), Seasonal migration of ITCZ precipitation across the equator: Why can't GCMs simulate it?, *Geophys. Res. Lett.*, *30*(15), 1824, doi:10.1029/2003GL017198.
Xie, S., M. Zhang, J. S. Boyle, R. T. Cederwall, G. L. Potter, and W. Lin (2004), Impact of a revised convective triggering mechanism on Community Atmosphere Model, Version 2, simulations: Results from short-range weather forecasts, *J. Geophys. Res.*, *109*, D14102, doi:10.1029/2004JD004692.
Xu, K.-M., and D. A. Randall (1996), A semiempirical cloudiness parameterization for use in climate models, *J. Atmos. Sci.*, *53*, 3084–3102.
Yang, B., Y. Qian, G. Lin, R. Leung, and Y. Zhang (2012), Some issues in uncertainty quantification and parameter tuning: A case study of convective parameterization scheme in the WRF regional climate model, *Atmos. Chem. Phys.*, *12*, 2409–2427, doi:10.5194/acp-12-2409-2012.
Yang, B., et al. (2013), Uncertainty quantification and parameter tuning in the CAM5 Zhang-McFarlane convection scheme and impact of improved convection on the global circulation and climate, *J. Geophys. Res.*, *118*, 395–415, doi:10.1029/2012JD018213.
Yang, G.-Y., and J. Slingo (2001), The diurnal cycle in the tropics, *Mon. Weather Rev.*, *129*, 784–801.
Yano, J.-I., M. Bister, Ž. Fuchs, L. Gerard, V. T. J. Phillips, S. Barkidija, and J.-M. Piriou (2013), Phenomenology of convection-parameterization closure, *Atmos. Chem. Phys.*, *13*, 4111–4131, doi:10.5194/acp-13-4111-2013.
Yuan, X., and X.-Z. Liang (2011), Evaluation of a Conjunctive Surface-Subsurface Process Model (CSSP) over the contiguous United States at regional-local scales, *J. Hyrdrometeorol.*, *12*, 579–599, doi:10.1175/2010JHM1302.1.
Zhang, G. J. (2003), Roles of tropospheric and boundary layer forcing in the diurnal cycle of convection in the U.S. southern great plains, *Geophys. Res. Lett.*, *30*(24), 2281, doi:10.1029/2003GL018554.
Zhang, G. J., and N. A. McFarlane (1995), Sensitivity of climate simulations to the parameterization of cumulus convection in the Canadian Climate Centre general circulation model, *Atmos. Ocean*, *33*, 407–446.
Zhang, G. J., and M. Mu (2005), Effects of modifications to the Zhang-McFarlane convection parameterization on the simulation of the tropical precipitation in the National Center for Atmospheric Research Community Climate Model, version 3, *J. Geophys. Res.*, *110*, D09109, doi:10.1029/2004JD005617.
Zhang, G. J., and H. Wang (2006), Toward mitigating the double ITCZ problem in NCAR CCSM3, *Geophys. Res. Lett.*, *33*, L06709, doi:10.1029/2005GL025229.
Zhou, L., and Y. Wang (2006), Tropical rainfall measuring mission observation and regional model study of precipitation diurnal cycle in the New Guinean region, *J. Geophys. Res.*, *111*, D17104, doi:10.1029/2006JD007243.